ELASTIC ANALYSIS OF A CIRCUMFERENTIAL CRACK IN AN ISOTROPIC CURVED BEAM USING MODIFIED MAPPING-COLLOCATION METHOD

A THESIS SUBMITTED TO
THE GRADUATE SCHOOL OF NATURAL AND APPLIED SCIENCES
OF
MIDDLE EAST TECHNICAL UNIVERSITY

AYDIN AMIREGHBALI

IN PARTIAL FULFILLMENT OF THE REQUIREMENTS
FOR
THE DEGREE OF MASTER OF SCIENCE
IN
AEROSPACE ENGINEERING

FEBRUARY 2013

Approval of the thesis:

ELASTIC ANALYSIS OF A CIRCUMFERENTIAL CRACK IN AN ISOTROPIC CURVED BEAM USING MODIFIED MAPPING-COLLOCATION METHOD

submitted by **AYDIN AMIREGHBALI** in partial fulfillment of the requirements for the degree of **Master of Science in Aerospace Engineering Department, Middle East Technical University** by,

Prof. Dr. Canan Özgen
Dean, Graduate School of **Natural and Applied Sciences**

Prof. Dr. Ozan Tekinalp
Head of Department, **Aerospace Engineering**

Assist. Prof. Dr. Demirkan Çöker
Supervisor, **Aerospace Engineering Department, METU**

Examining Committee Members:

Prof. Dr. Altan Kayran
Aerospace Engineering Department, METU

Assist. Prof. Dr. Demirkan Çöker
Aerospace Engineering Department, METU

Prof. Dr. Ozan Tekinalp
Aerospace Engineering Department, METU

Assoc. Prof. Dr. Serkan Dağ
Mechanical Engineering Department, METU

Assist. Prof. Dr. Ercan Gürses
Aerospace Engineering Department, METU

Date:

I hereby declare that all information in this document has been obtained and presented in accordance with academic rules and ethical conduct. I also declare that, as required by these rules and conduct, I have fully cited and referenced all material and results that are not original to this work.

Name, Last Name: AYDIN AMIREGHBALI

Signature :

ABSTRACT

ELASTIC ANALYSIS OF A CIRCUMFERENTIAL CRACK IN AN ISOTROPIC CURVED BEAM USING MODIFIED MAPPING-COLLOCATION METHOD

Amireghbali, Aydin
M.Sc., Department of Aerospace Engineering
Supervisor : Assist. Prof. Dr. Demirkan Çöker

February 2013, 55 pages

The modified mapping-collocation (MMC) method is applied to analyze a circumferential crack in an isotropic curved beam. Based on the method a MATLAB code was developed to obtain the stress field. Incorporating the stress correlation technique, the opening and sliding fracture mode stress intensity factors (SIF)s of the crack for the beam under pure bending moment load case are calculated.

The MMC method aims to solve two-dimensional problems of linear elastic fracture mechanics (LEFM) by combining the power of analytic tools of complex analysis (Muskhelishvili's formulations, conformal mapping, and extension arguments) with simplicity of applying the boundary collocation method as a numerical solution approach.

Qualitatively, a good agreement between the computed stress contours and the fringe shapes obtained from the photoelastic experiment on a plexiglass specimen is observed. Quantitatively, the results are compared with that of ANSYS finite element analysis software. The effect of crack size, crack position and beam thickness variation on SIF values and mode mixity is investigated.

Keywords: linear elastic fracture mechanics (LEFM), modified mapping-collocation (MMC) method, stress intensity factor (SIF), circumferential crack, curved beam, pure bending, complex analysis, conformal mapping, Muskhelishvili formulation, boundary collocation method, stress correlation technique, ANSYS Mechanical APDL

ÖZ

MODİFİYE HARİTALAMA-EŞDİZİMLİLİK YÖNTEMİ İLE İZOTROPİK EĞRİ KİRİŞ İÇİNDEKİ ÇEVRERSEL ÇATLAĞIN ELASTİK ANALİZİ

Amireghbali, Aydin
Yüksek Lisans, Havacılık ve Uzay Mühendisliği Bölümü
Tez Yöneticisi : Yrd. Doç. Dr. Demirkan Çöker

Şubat 2013 , 55 sayfa

İzotropik eğri kirişteki çevresel çatlağın elastik analizi için modifiye haritalama-eşdizimlilik (MMC) yöntemi uygulanmıştır. Yöntemi saf bükme yükü altında olan bu nesne için kullanmak üzere MATLAB kodu geliştirerek; gerilme alanı elde edilmiştir. Gerilme bağıntı tekniğini yönteme katarak çatlağın açılma ve kayma kırılma modları için gerilme şiddeti faktörü (SIF) değerleri hesaplanmıştır.

İki-boyutlu linear elastik kırılma mekaniği problemlerin çözümünü amaçlayan MMC yöntemi, kompleks analiz teorisinin analitik araçlarının (Muskhelishvili formülasyonu, açı-korur haritalama ve genişletme argümanları) gücünü sınır eşdizimlilik metodunun nümerik uygulanma kolaylığı ile birleştiriyor.

Hesaplanmış olan eşyükselti gerilme eğrilerin, pleksiglas numune üzerindeki fotoelastik deneyin frinç şekilleri ile nitel uyumu gözlemlenmiştir. ANSYS sonlu elemanlar yazılımı sonuçları ile karşılaştırarak nicel uyum araştırılmıştır. Çatlak büyüklüğü, konumu, ve kiriş kalınlığının SIF'ler ve onların oranı üzerindeki etkisi incelenmiştir.

Anahtar Kelimeler: linear elastik kırılma mekaniği (LEFM), modifiye haritalama-eşdizimlilik (MMC) yöntemi, gerilme şiddeti faktörü (SIF), çevresel çatlak, eğri kiriş, saf bükme yükü, kompleks analiz, açı-korur haritalama, Muskhelishvili formülasyonu, sınır eşdizimlilik metodu, gerilme bağıntı tekniği, ANSYS Mechanical APDL

To my family, whom I met little during these years

ACKNOWLEDGMENTS

I would like to express my sincere gratitude to my thesis supervisor, Professor Demirkan Coker, whom this work would not have been possible without his superior guidance and also encouragement.

I am deeply grateful to Professor Alan Zehnder for his brilliantly helpful non-profit ebook [3].

My thanks also goes to the fellows who shared with me their office at the hangar building for over a year; namely, friends of mine, Denizhan Yavas, for the photoelastic test result (Figure 3.1-(b)) and Miray Aydan Arca, Imren Uyar and Basar Kutukoglu, for their immense help on enhancing my thesis defense presentation manner.

Words are inadequate in offering my thanks to Mrs. Michelle Krummel, whose unique introduction of the Texmaker editor [26] is highly recommended to everyone who starts learning LaTeX.

Finally; I wish to thank my parents, to whom I am indebted forever for all of their support.

TABLE OF CONTENTS

ABSTRACT v

ÖZ vi

ACKNOWLEDGMENTS viii

TABLE OF CONTENTS ix

LIST OF TABLES xii

LIST OF FIGURES xiii

LIST OF SYMBOLS AND ABBREVIATIONS xvi

CHAPTERS

1 INTRODUCTION 1

1.1 The problem perspective 1

1.2 The MMC method, the big picture 3

1.3 Literature Survey 4

2 FORMULATION AND SOLUTION 5

2.1 Stress boundary condition equations 5

2.2 Force boundary condition equations 7

2.3 Moment boundary condition equations 8

2.4 The solution procedure 9

3 RESULTS AND CONCLUSIONS 11

3.1 Results 11
3.1.1 Versus photoelastic caustics 12
3.1.2 Versus FEA 13
3.1.3 Accuracy 13
3.1.4 Parametric study 16
3.1.4.1 The crack position effect 17
3.1.4.2 The beam thickness effect 17
3.2 Conclusions 20
REFERENCES 23
APPENDICES
A MUSKHELISHVILI'S COMPLEX REPRESENTATIONS 25
A.1 The stress function 25
A.2 Stress field equations 27
A.3 Stress boundary condition equations 28
A.4 Force boundary condition equations 30
A.5 Moment boundary condition equation 31
B CONFORMAL MAPPING AND ITS AIM 33
B.1 The mapping function 33
B.2 Kartzivadze's continuation argument 34
C THE LAURENT SERIES REPRESENTATION 37
C.1 The Laurent series 37
C.2 The effect of stress symmetry 37
D PURE BENDING OF A CURVED BEAM 43

D.1 The equivalent stress distribution 43

D.2 Force resultants 44

D.3 Moments 45

E ANSYS PROCEDURES 47

E.1 Modelling 48

E.2 Meshing 48

E.3 Applying the boundary conditions 50

E.4 Solving and plotting 51

E.5 Reading and listing the stress values 52

E.6 Calculating SIFs via displacement extrapolation method 54

LIST OF TABLES

TABLES

Table E.1 The force components applied to the nodes (in Newtons) 50

LIST OF FIGURES

FIGURES

Figure 1.1 ASTM D6415 test apparatus and specimen configuration. The grey part is of prime concern. 2

Figure 1.2 The curved beam with circumferential crack 2

Figure 1.3 Two curved beams attached *partially* by a weak interface, under 4-point bending 3

Figure 2.1 On the unit circle 7

Figure 3.1 The maximum shear stress contours for the *sample beam* according to the: (a) MATLAB code applying the MMC method (b) photoelastic test of plexiglass specimen, courtesy of Denizhan Yavas 12

Figure 3.2 Stress variation on the arc that includes the crack for the *sample beam* . . . 12

Figure 3.3 *Stress intensity* $(2 * \tau_{max})$ contours for the half sample beam containing a crack of $\beta = 25°$ at $h_a = 0.5$ obtained from (a) MATLAB code applying the MMC method and (b) ANSYS FEA 14

Figure 3.4 *Stress intensity* $(2 * \tau_{max})$ contours in 1 cm^2 vicinity of the crack-tip for the half sample beam containing a crack of $\beta = 25°$ at $h_a = 0.5$ obtained from (a) MATLAB code applying the MMC method and (b) ANSYS FEA 15

Figure 3.5 Deviation from the classical solution for normal stress distribution on the moment-exerted boundary for the *sample beam* with different β values 16

Figure 3.6 The markers represesnt the MMC method recalculated stresses in polar coordinates, the lines show the corresponding stress components extracted from ANSYS, both plotted for the points on a $20°$ arc with its center at the origin of the xy plane which has the crack tip at its midpoint and includes $10°$ of the crack surface 17

Figure 3.7 (a) Non-dimensionalized mode-I SIF and (b) Mode-mixity, versus crack half arc angle, β, for different crack positions $h_a = 0.25, 0.5$ and 0.75 for the beam with $R_1 = 15mm$ and $R_2 = 45mm$ for which the non-dimensionalising stress value is $\sigma = (\sigma_\theta)_{r=R_1} = 10.2MPa$ 18

Figure 3.8 (a) Non-dimensionalized mode-I SIF and (b) Mode-mixity, versus crack half arc angle, β, for a central crack ($h_a = 0.5$) at $R_a = 30mm$, in beams of $t = 10, 20$ and $30mm$ thickness, for which corresponding non-dimensionalising stress values are $\sigma = (\sigma_\theta)_{r=R_1} = 67.6, 19.4$ and $10.2MPa$ respectively 19

Figure 3.9 Mode-I SIF (K_I) versus crack half arc angle, β, for a central crack ($h_a = 0.5$) at $R_a = 30mm$ in beams of different thicknesses $t = 10,\ 20$ and $30mm$ 20

Figure A.1 The axes of element stress transformation 28

Figure A.2 The normal and tangential traction components 29

Figure A.3 An infinitesimal element on the boundary 30

Figure B.1 The successive mapping plan 34

Figure B.2 The unit circle interior, and exterior 35

Figure C.1 The *punctured region*'s symmetry and mirrored shear stress 39

Figure D.1 The opening couple and its equivalent stress distribution 44

Figure D.2 The stress traction vector on the moment-exerted end of the beam 45

Figure D.3 The force components on the moment-exerted end of the beam 45

Figure E.1 The half-beam ANSYS *model* 49

Figure E.2 The boundary conditions applied on the body and a close view of the crack-tip vicinity mesh, where two rows of singular elements are generated 51

Figure E.3 An alternative finite element modelling strategy 52

Figure E.4 The local x-y coordinate system and the path definition order 55

LIST OF SYMBOLS AND ABBREVIATIONS

α Beam half arc angle (alpha equals $\frac{\pi}{4}$)

β Crack half arc angle (beta)

ζ Complex variable in the image region (zeta)

θ Angular coordinate (theta)

σ Stress component (sigma)

τ Shear stress (tau)

ϕ Analytic complex function (phi)

χ Analytic complex function (chi)

ψ Analytic complex function (psi)

Ω Kolosov complex expression for $\sigma_y - \sigma_x + i\sigma_{xy}$ (Omega)

ω complex term in Ω (omega)

∇ Del (or gradient vector) operator (Nabla symbol)

∇^2 Laplace operator (Laplacian)

$\Im$ Imaginary part

$\Re$ Real part

A Purely real coefficients of the Laurent series, Boundary point, Coefficients matrix

a Complex coefficients of the Laurent series coefficient, Crack

APDL ANSYS parametric design language

ASTM American society for testing and materials

B Boundary point

b Beam width in z-direction, column matrix of constants

bar (overbar) Conjugate of a complex variable or function

C Boundary point

c Center (origin) of the coordinate system

CFRP Carbon fibre reinforced polymer

e Euler's number (equals 2.71828)

exp Exponential function

F Analytic complex function

f Analytic complex function

$f(w)$ Complex mapping function

FEA Finite elements analysis

fn Complex function

g Analytic complex function

$g(\zeta)$ Complex mapping function

H Non-dimensionalized stress intensity factor

h Analytic complex function

$h(\zeta)$ Composite complex mapping function

h_a Crack position ($h_a = \frac{R_a - R_1}{R_2 - R_1}$)

I Opening fracture mode

i Imaginary unit

II Sliding fracture mode

K Stress intensity factor

L Straight crack length in the auxiliary w-plane

LFEM Linear elastic fracture mechanics

M Moment, Lower index of the Laurent series

m mean

MMC Modified mapping collocation

N Normal component of stress traction on boundary, Upper index of the Laurent series

n The Laurent series index

N_G Golovin expression (see equation (2.13))

P Analytic complex function

p Analytic complex function

Q Analytic complex function

q Analytic complex function

R_1 Beam inner radius

R_2 Beam outer radius

R_a Crack radius

RMS Root mean square

r Radial coordinate (distance)

s Boundary

SIF Stress intensity factor

T Tangential component of stress traction on boundary, Stress traction vector on boundary

t Beam thickness ($t = R_2 - R_1$)

U Airy stress function

w Complex variable in the auxiliary plane

x The physical plane real axis

y The physical plane imaginary axis

x' Rotated x axis

y' Rotated y axis

z Complex variable in the physical plane, Coordinate perpendicular to xy plane

CHAPTER 1

INTRODUCTION

Delamination (or interlaminar fracture) as a mechanism of failure in laminated composite materials is a current source of manufacturing quality issue in aerospace and wind turbine industries and of high importance to prevent damage to the composite airframe parts. Generally occurring before other modes of damage, it causes *the weakest link* (resistance to de-cohesion among laminae) to determine the ability to bear load. The phenomenon is not only of high importance because of probable safety problems it may cause, but also in regard to effects of its consideration in design procedure on costs through body weight and material consumption.

For thin-walled aircraft structures, stresses normal to the laminated panels are usually very low and therefore of no concern, however, for curved laminated parts, interlaminar tensile stresses become quite large. For example consider the A400M Airbus wingbox, which is a fuel tank. The "C"-section CFRP (carbon fiber reinforced polymer) spars are bolted to the skin and engulf the tanks. A critical load case for A400M is a refuel overflow, during which a fault causes tanks to become over-filled, creating a large rise in the tank internal pressure. This develops an opening moment and the spar corners begin to experience significant through-thickness tensile stresses among the plies within the laminate [1].

The standard test method established by ASTM [2], aims at determination of the curved beam strength of a continuous fiber-reinforced composite material using a 90° curved beam specimen (Figure 1.1). Especially designed for through-the-thickness interlaminar tensile stress measurements, it is emphasized by the standard that *the failure should be carefully observed to ensure that a delamination(s) is produced across the width before the failure data are used.*

According to linear elastic fracture mechanics (LEFM) theory, the stress field around the crack tip could be represented by a single quantity defined as the stress intensity factor (SIF). For each mode of opening or sliding, it uniquely reflects loading and geometry of the cracked component. When this quantity reaches its critical value (fracture toughness of the material), the crack starts to grow. SIF vales are of fundamental concern in fracture mechanics studies.

1.1 The problem perspective

The present study of a circumferential crack in an isotropic curved beam subjected to pure bending moment (Figure 1.2), beside beating a path for application of the MMC method to the problem of orthotropic case, provides the opportunity of comparing the solution results with that of a specimen composed of two isotropic beams glued at interface, with a partial

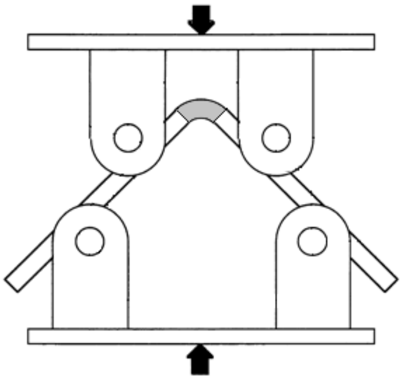

Figure 1.1: ASTM D6415 test apparatus and specimen configuration. The grey part is of prime concern.

no-glue region as pre-crack (see Figure 1.3). This also supplies a rough estimation of that to what extent a homogeneously orthotropic (no-interface) body with a crack could mimic delamination in laminated composites in the later studies.

Curved laminated composite beams are frequently used in aero-structures and wind turbine blades. The present work is a first step for future study of the possibility of modelling delamination in these structural parts by considering a circumferential crack in a homogeneous cylindrically orthotropic model. In this step, it is *presumed* that while there is no crack growth, a one-piece isotropic curved beam which contains a circumferential crack (Figure 1.2), simulates a specimen including two isotropic curved beams attached partially by a weak interface, where the glue-free part stands as a pre-crack (Figure 1.3). In other words, it is assumed that the problem under investigation, composes a reasonable model for the case with glued interface.

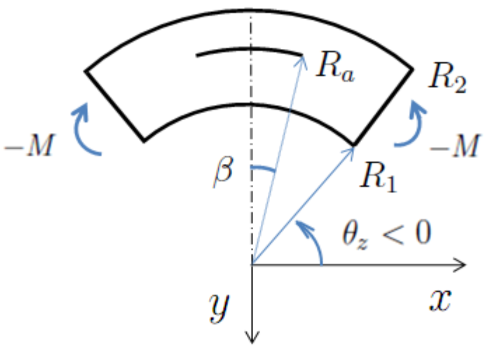

Figure 1.2: The curved beam with circumferential crack

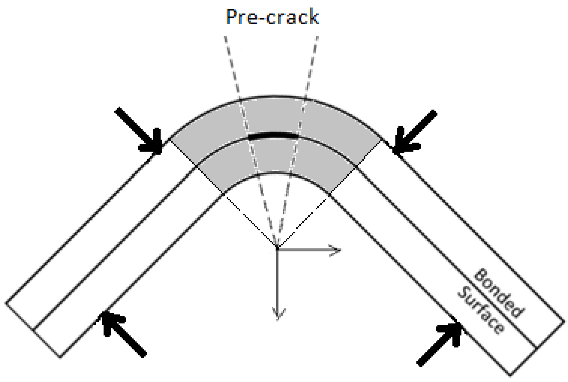

Figure 1.3: Two curved beams attached *partially* by a weak interface, under 4-point bending

1.2 The MMC method, the big picture

In the current study, the MMC method is applied in order to obtain SIFs for both opening and sliding modes of a circumferential crack in an isotropic curved beam under pure bending. The effect of crack size, crack radius and beam thickness on SIFs is studied by developing a MATLAB code. The calculated stress field maximum shear contours, near (and far away from) crack tip, are plotted.

The modified mapping collocation (MMC) method is a semi-analytic approach to solve boundary value problems of 2-D LEFM. The analytical part, makes use of complex analysis tools to reduce the boundary condition equations into a linear system of equations which its unknowns are the stress function series expansion coefficients. The numerical part of the method takes advantage of boundary collocation method to solve the overdetermined system of equations supplied by the analytic part in a least-square sense.

As a method developed to treat two-dimensional fracture mechanics problems, the objective of MMC method is the calculation of SIFs; however, solving the fundamental boundary value problem of two-dimensional elasticity (circumventing the need for direct treatment of the biharmonic equation), it primarily provides the stress function and therefore the stress field near (and also far away from) the crack tip. Then it is an easy matter to calculate SIF values, using the *stress correlation* technique [3].

According to G. V. Kolosov [4], only two analytic complex functions (e.g. $\phi(z)$ and $\psi(z)$) are sufficient to fully describe the stress field in a two-dimensional elastic body. The boundary condition equations was written by N. I. Muskhelishvili [4] in terms of these two analytic complex functions (see Appendix A). The advantages of performing conformal mapping and applying extension arguments become more clear when dealing with cracked body problems. Finding a proper mapping function, which maps the unit circle in the image plane into the crack in the physical plane, and using extension arguments; the traction-free condition on the crack surface can be satisfied analytically (Appendix B). Besides, the number of analytic functions needed reduces to one (as one can be expressed in terms of the other). Finally, a suitable ground for applying the Laurent theorem and series to the problem emerges in the image region (Appendix C).

1.3 Literature Survey

The MMC method was introduced by O. L. Bowie in 1970 as an accurate method to calculate SIFs for isotropic two-dimensional LEFM problems. In his paper [5] the method is applied to the problem of a circular disk containing an internal straight crack under uniform external tension upon its perimeter.

Later developed further for orthotropic problems [6], the method was applied to a range of isotropic two-dimensional problems, all with straight cracks; for a radial crack in a circular ring [7], for a radial crack in a segment of a circular ring [8] and for radial cracks emanating from both inner and outer surfaces of a circular ring [9].

The analytic part of the method is mainly based on the comprehensive work of N. I. Muskhelishvili [4], in which his complex representations for boundary condition equations, besides conformal mapping and extension (or continuation) arguments of both Muskhelishvili and Kartzivadze are introduced and applied to the two-dimensional LEFM problems.

CHAPTER 2

FORMULATION AND SOLUTION

According to Muskhelishvili's complex representations (Appendix A); stress, force and moment boundary condition equations can be written in terms of two *analytic* complex functions (e.g. $\phi(z)$ and $\psi(z)$) in the physical plane. By using a proper mapping function and taking advantage of the *continuation* concept (Appendix B), it becomes possible to write the boundary condition equations in terms of only one analytic function in the image plane (i.e. solely $\phi(\zeta)$). In addition, applying Kartzivadze's continuation argument makes the so-called *traction free* conditions on the crack surfaces satisfied analytically.

Thus, to find the stress field, it is sufficient to find $\phi(\zeta)$. Assuming a Laurent series expansion for $\phi(\zeta)$ (Appendix C), the boundary condition at each point ζ on the boundary becomes a linear equation which its unknowns are coefficients of the series.

Stress, force and moment at each boundary point (i.e. right hand side values of the acquired linear equations) can be obtained on the basis of Golovin's solution (Appendix D). These *crack-less* curved beam values, are supplied to the equations to solve the cracked case. This is assumed that the results should be reasonable as long as the crack is not *so large*.

In the subsequent sections the boundary condition equations are transformed from the physical z-plane into the image ζ-plane, where by substituting the Laurent series expansion of $\phi(\zeta)$, the equations can be expressed as linear equations in terms of ζ. The series expansion coefficients are unknowns of the constructed system of equations.

The intendedly overdetermined system of boundary condition equations is to be solved in a least square sense. Determination of $\phi(\zeta)$ leads to determination stress field. Thereafter stress correlation technique can be used to calculate SIF values. The final section explains the solution procedure indicating the applied MATLAB functions.

2.1 Stress boundary condition equations

According to Appendix A, equation (A.46):

$$\phi'(z) + \overline{\phi'(z)} - [\bar{z}\phi''(z) + \psi'(z)]e^{2i\theta} = N - iT \tag{2.1}$$

where N and T stands for normal and tangential components of stress traction at boundary point and θ is the angle N makes with positive direction of x axis (see Figure A.2). The bar represents conjugate function.

Considering the mapping function to be (see Appendix B):

$$z = h(\zeta) = R_a \exp\{i[\frac{\beta}{2}(\zeta + \zeta^{-1}) - \frac{\pi}{2}]\} \tag{2.2}$$

where R_a is crack radius and β is crack half-arc angle.

Defining:

$$\phi(z) = \phi[h(\zeta)] = \phi_1(\zeta) \tag{2.3}$$

due to the *chain rule*:

$$\phi'(z) = \frac{d\phi(z)}{dz} = \frac{d\phi_1(\zeta)}{d\zeta} \cdot \frac{d\zeta}{dz} = \frac{\phi_1'(\zeta)}{h'(\zeta)} \tag{2.4}$$

consequently:

$$\phi''(z) = \frac{d}{dz}(\frac{\phi_1'(\zeta)}{h'(\zeta)}) = \frac{d}{d\zeta}(\frac{\phi_1'(\zeta)}{h'(\zeta)}) \cdot \frac{d\zeta}{dz} \tag{2.5}$$

$$\phi''(z) = \frac{\phi_1''(\zeta).h'(\zeta) - \phi_1'(\zeta).h''(\zeta)}{[h'(\zeta)]^2} / \frac{dh(\zeta)}{d\zeta} \tag{2.6}$$

$$\phi''(z) = \frac{h'(\zeta).\phi_1''(\zeta) - h''(\zeta).\phi_1'(\zeta)}{[h'(\zeta)]^3} \tag{2.7}$$

Similar to (2.3) and (2.4):

$$\psi(z) = \psi[h(\zeta)] = \psi_1(\zeta) \tag{2.8}$$

$$\psi'(z) = \frac{d\psi(z)}{dz} = \frac{d\psi_1(\zeta)}{d\zeta} \cdot \frac{d\zeta}{dz} = \frac{\psi_1'(\zeta)}{h'(\zeta)} \tag{2.9}$$

As a result of Kartzivadze's continuation argument (appendix B, section B.2):

$$\psi_1(\zeta) = -\overline{\phi_1}(\frac{1}{\zeta}) - \frac{\overline{h}(\frac{1}{\zeta})}{h'(\zeta)}\phi_1'(\zeta), \qquad for\ |\zeta| > 1 \tag{2.10}$$

differentiating the above equation with respect to ζ and substituting into (2.9), left hand side (2.1) can be obtained in terms of $\phi(\zeta)$ only (see section C.2, equations (C.2)-(C.5) for the details).

In addition, Appendix C asserts that:

$$\phi_1(\zeta) = \sum_n [iA_{2n}\zeta^{2n} + A_{2n+1}\zeta^{2n+1}] \tag{2.11}$$

where A_{2n} and A_{2n+1} are purely real, takes into account the stress symmetry of the problem with respect to the imaginary axis.

The boundary conditions require T to be zero everywhere on the boundary. The same thing is required for N except on the moment-exerted ends of the beam where $N \equiv \sigma_\theta(r)$ and is given by Golovin's solution (Figure D.1):

$$\sigma_\theta(r) = -\frac{4M}{N_G b}[-\frac{R_1^2 R_2^2}{r^2}\ln(\frac{R_2}{R_1}) + R_2^2\ln(\frac{r}{R_2}) + R_1^2\ln(\frac{R_1}{r}) + R_2^2 - R_1^2] \tag{2.12}$$

where:

$$N_G = (R_2^2 - R_1^2)^2 - 4R_1^2R_2^2(\ln(\frac{R_2}{R_1}))^2 \tag{2.13}$$

where M is absolute value of the moment exerted, b stands for depth of the beam in z-direction and R_1 and R_2 are inner and outer radii of the beam.

Putting all together, equation (2.1) produces two linear equations at each boundary point, one for tangential component of stress traction and the other for normal component of that vector (by its real and imaginary parts respectively). The unknowns are A_{2n} and A_{2n+1} (i.e. purely real coefficients of the Laurent series expansion (2.11)).

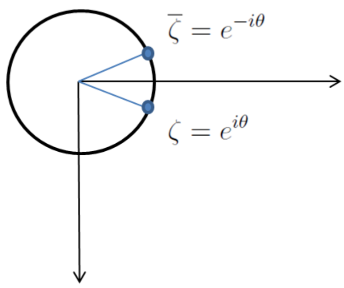

Figure 2.1: The unit circle, ζ and $\overline{\zeta}$

2.2 Force boundary condition equations

The force boundary condition equations obtained in Appendix A as:

$$b.i[\phi(z) + z\overline{\phi'(z)} + \overline{\psi(z)}]_{z_A}^{z_B} = (F_x + iF_y)_{on\ \overline{AB}} \tag{2.14}$$

The right hand side expression is shown (Appendix D) to be given by:

$$(F_x + iF_y)_{on\ \overline{AB}} = -[\cos(\alpha) + i\sin(\alpha)] \cdot \frac{4M}{N_G}[R_1^2 r\ln(\frac{R_1}{r}) + R_2^2 r\ln(\frac{r}{R_2}) + \frac{R_1^2R_2^2}{r}\ln(\frac{R_2}{R_1})]_{r_A}^{r_B} \tag{2.15}$$

substituting this into above and multiplying both by $-i/b$:

$$[\phi(z) + z\overline{\phi'(z)} + \overline{\psi(z)}]_{z_A}^{z_B} = \frac{1}{b}[i\cos(\alpha) - \sin(\alpha)]\frac{4M}{N_G}[R_1^2 r\ln(\frac{R_1}{r}) + R_2^2 r\ln(\frac{r}{R_2}) + \frac{R_1^2R_2^2}{r}\ln(\frac{R_2}{R_1})]_{r_A}^{r_B} \tag{2.16}$$

Using $z = h(\zeta)$ (equation (2.2)), the left hand side can be transferred into the ζ-plane. Considering (2.4):

$$\overline{\phi'(z)} = \frac{\overline{\phi_1'(\zeta)}}{\overline{h'(\zeta)}} \tag{2.17}$$

Besides, taking conjugate of (2.10):

$$\overline{\psi_1(\zeta)} = -\phi_1(\frac{1}{\overline{\zeta}}) - \frac{h(\frac{1}{\overline{\zeta}})}{\overline{h'(\zeta)}}\overline{\phi_1'(\zeta)}, \qquad for\ |\zeta| > 1 \tag{2.18}$$

substituting into left hand side (2.16) it may be rewritten as:

$$[\phi(z) + z\overline{\phi'(z)} + \overline{\psi(z)}]_{z_A}^{z_B} = [\phi_1(\zeta) - \phi_1(\frac{1}{\overline{\zeta}}) + (h(\zeta) - h(\frac{1}{\overline{\zeta}}))\frac{\overline{\phi_1'(\zeta)}}{\overline{h'(\zeta)}}]_{\zeta_A}^{\zeta_B} \tag{2.19}$$

Note that since on a unit circle ($\zeta = \exp(i\theta)$), we have $\zeta = \frac{1}{\overline{\zeta}}$, (see Figure 2.1) it can be seen from right hand side of the force boundary equation (above) that so-called traction free condition on crack is satisfied automatically.

Substituting (2.19) into (2.16):

$$[\phi_1(\zeta) - \phi_1(\frac{1}{\overline{\zeta}}) + (h(\zeta) - h(\frac{1}{\overline{\zeta}}))\frac{\overline{\phi_1'(\zeta)}}{\overline{h'(\zeta)}}]_{\zeta_A}^{\zeta_B} =$$

$$(i\cos(\alpha) - \sin(\alpha))\frac{4M}{N_G b}[R_1^2 r\ln(\frac{R_1}{r}) + R_2^2 r\ln(\frac{r}{R_2}) + \frac{R_1^2R_2^2}{r}\ln(\frac{R_2}{R_1})]_{r_A}^{r_B} \tag{2.20}$$

This is the force equation on the moment-exerted end of the beam, however on traction free faces one finds:

$$[\phi_1(\zeta) - \phi_1(\frac{1}{\overline{\zeta}}) + (h(\zeta) - h(\frac{1}{\overline{\zeta}}))\frac{\overline{\phi_1'(\zeta)}}{\overline{h'(\zeta)}}]_{\zeta_A}^{\zeta_B} = 0 \tag{2.21}$$

where $\phi_1(\zeta)$ is to be expanded as given in (2.11). Hence at each boundary point there are two equations due to real and imaginary parts of (2.20) and (2.21).

2.3 Moment boundary condition equations

The moment boundary equation in the physical plane obtained as (Appendix A):

$$\Re\{[z\bar{z}\phi'(z) + z\psi(z) - \chi(z)]_{z_A}^{z_B}\} = (M_z)_{on\ \overline{AB}} \tag{2.22}$$

where:

$$\chi(z) = \int \psi(z)dz \tag{2.23}$$

Considering (2.8) and noting $z = h(\zeta)$, the above equation is rewritten as:

$$\chi(\zeta) = \int \psi_1(\zeta)d(h(\zeta)) \tag{2.24}$$

multiplying and dividing the integrand by $d\zeta$:

$$\chi(\zeta) = \int \psi_1(\zeta).h'(\zeta)d\zeta \tag{2.25}$$

substituting $\psi_1\zeta)$ from (2.10):

$$\chi(\zeta) = -\int [h'(\zeta).\overline{\phi}(\frac{1}{\zeta}) + \overline{h}(\frac{1}{\zeta}).\phi'(\zeta)]d\zeta \tag{2.26}$$

substituting (2.26),(2.4) and (2.10) into (2.22):

$$\begin{aligned} &- \quad \Re\{\int_{\zeta_A}^{\zeta_B} [h'(\zeta).\overline{\phi}(\frac{1}{\zeta}) + \overline{h}(\frac{1}{\zeta}).\phi'(\zeta)]d\zeta\} \\ &- \quad \Re\{[h(\zeta).\overline{h(\zeta)} \cdot \frac{\phi'(\zeta)}{h'(\zeta)}]_{\zeta_A}^{\zeta_B}\} \\ &- \quad \Re\{[h(\zeta).\overline{\phi}(\frac{1}{\zeta}) + \frac{h(\zeta).\overline{h}(\frac{1}{\zeta})}{h'(\zeta)}\phi'(\zeta)]_{\zeta_A}^{\zeta_B}\} = (M_z)_{on\ \overline{AB}} \end{aligned} \tag{2.27}$$

changing integration limits with each other and reordering:

$$\Re\{\int_{\zeta_B}^{\zeta_A} [h'(\zeta).\overline{\phi}(\frac{1}{\zeta})+\overline{h}(\frac{1}{\zeta}).\phi'(\zeta)]d\zeta + [h(\zeta)\cdot(\frac{\overline{h(\zeta)} + \overline{h}(\frac{1}{\zeta})}{h'(\zeta)}\phi'(\zeta)+\overline{\phi}(\frac{1}{\zeta})]_{\zeta_A}^{\zeta_B}\} = (M_z)_{on\ \overline{AB}} \tag{2.28}$$

only the real part of the equation is needed to yield the moment equation corresponding to each boundary point (center of AB).

The right hand side value (M_z) is shown in Appendix D to be:

$$(M_z)_c = |\Im\{z_c\}|.F_x + |\Re\{z_c\}|.F_y \tag{2.29}$$

where F_x and F_y can be obtained from (2.15).

2.4 The solution procedure

The MMC method advices construction of a system of linear (boundary condition) which intendedly has more equations than unknowns (i.e is an *overdetermined* system). For this purpose, MATLAB *Symbolic Toolbox* was used to substitute the expressions corresponding to the $\phi(\zeta)$ function (based on expansion (2.11)) into the boundary condition equations. These expressions are $\phi^{'}(\zeta)$, $\phi^{''}(\zeta)$ and $\overline{\phi}^{'}(\frac{1}{\zeta})$, and their expanded forms are given in Appendix C. Then boundary condition equations are written (evaluated) at discrete collocation points (stations) on the boundary. At each station on the boundary, two linear stress boundary condition equations (considering real and imaginary parts of the complex equation) are obtained. For the force and moment equations the process is a little different since they are evaluated between every two successive stations (A and B) on the boundary. Finally the process ends up with construction of a linear system of equations which its unknowns are coefficients of the $\phi(\zeta)$ function Laurent series expansion.

The overdetermined system of linear (boundary condition) equations is constructed by writing the equations for discrete points (stations) on the boundary. On the inner radius, the moment-exerted and the outer radius boundaries 3, 4 and 5 stations are considered respectively. For the Laurent series expansion (equation (2.11)), M and N values both were set to 3. The constructed overdetermined system is solved in a least square sense (using MATLAB `lsqr` function). The solution determines $\phi(\zeta)$ series expansion coefficients. Then the stress components at every point of the body can be found using Kolosov's formulae (A.33) and (A.35) in the image region:

$$\sigma_y + \sigma_x = 4\Re\{\frac{\phi^{'}(\zeta)}{h^{'}(\zeta)}\} \tag{2.30}$$

$$\sigma_y - \sigma_x + 2i\sigma_{xy} = 2\{\overline{h(\zeta)}\,\frac{h^{'}(\zeta)\phi^{''}(\zeta) - h^{''}(\zeta)\phi^{'}(\zeta)}{[h^{'}(\zeta)]^2} + \psi^{'}(\zeta)\}/h^{'}(\zeta) \tag{2.31}$$

Then, using stress correlation technique [3], SIFs are obtained by extrapolating (using MATLAB `interp1` function) the values in three points ahead and in vicinity of the crack tip considering that:

$$K_I = \lim_{r\to 0} \sqrt{2\pi r}\sigma_{22}(r,0) \tag{2.32}$$

$$K_{II} = \lim_{r\to 0} \sqrt{2\pi r}\sigma_{12}(r,0) \tag{2.33}$$

where I and II represent opening and sliding modes respectively and r stands for local radial distance from the crack tip and 1 and 2 represent directions tangential and perpendicular to the crack at its tip. In other words, since the stress filed is known, values of the expression in front of the *lim* operator (in each of the above cases) can be calculated and used for the extrapolation. The points are chosen on the line $\theta = 0$ (that is tangent to the crack at the crack tip) and are to be in an infinitesimal distance to the crack tip. The extrapolation of these values to $r = 0$ determines crack SIFs.

CHAPTER 3

RESULTS AND CONCLUSIONS

Considering the stress symmetry of the problem of *a circumferential crack in an isotropic curved beam under pure bending moment* with respect to the imaginary axis, the MMC method is applied successfully to the right hand side half of the curved beam.

Having determined $\phi(\zeta)$ series expansion coefficients from the linear system of boundary condition equations, stress values and thereafter SIF values (for both opening and sliding modes of fracture) are calculated.

The MMC-based MATLAB code result for the case study stress fringes is qualitatively compared with the photoelastic caustics obtained from the plexiglass specimen test with the same geometry. Also, a quantitative comparison is made between the stress field contours obtained from MATLAB and that of finite element analysis (FEA) using ANSYS Mechanical APDL (Appendix E). SIF values are evaluated using stress correlation technique (see section 2.4) incorporated to the MMC method. The recalculated stress on the beam boundaries is discussed as a measure of solution accuracy. The effects of different geometrical parameters on the SIF values are investigated.

3.1 Results

The results are separated into four parts. The first part contains a qualitative comparison between the MMC method stress field result with that of the photoelastic test for the same configuration, also stress state on the arc containing the crack is plotted. In the second part, the results of finite element analysis (FEA) done by ANSYS in terms of stresses, are compared with that brought up by MATLAB code applying the MMC method. In the third part, the stress distribution obtained from the MMC method is tackled as a measure of accuracy by comparing the values with that of the classical (crack-less) solution (Appendix D) and also with that of FEA. In the last part the SIF values (calculated according to the stress correlation technique (section 2.4)) are plotted as functions of crack and beam geometrical parameters. Obviously neither the mechanical properties nor the plane stress / plane strain assumptions are going to affect the results as long as only the stresses are of interest.

An opening moment of $-10Nm$ (i.e. $M = 10Nm$) is applied to and a width (b) of $0.01m$ is considered for all of the beams under investigation. Considering the symmetry of the problem with respect to the imaginary axis, the MMC method is applied successfully to one of the halves of the beam in order to find the stress field and thereafter opening and sliding mode

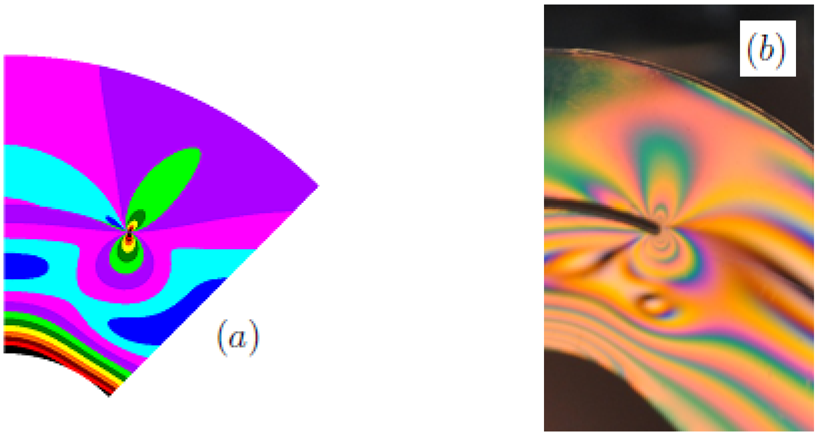

Figure 3.1: The maximum shear stress contours for the *sample beam* according to the: (a) MATLAB code applying the MMC method (b) photoelastic test of plexiglass specimen, courtesy of Denizhan Yavas

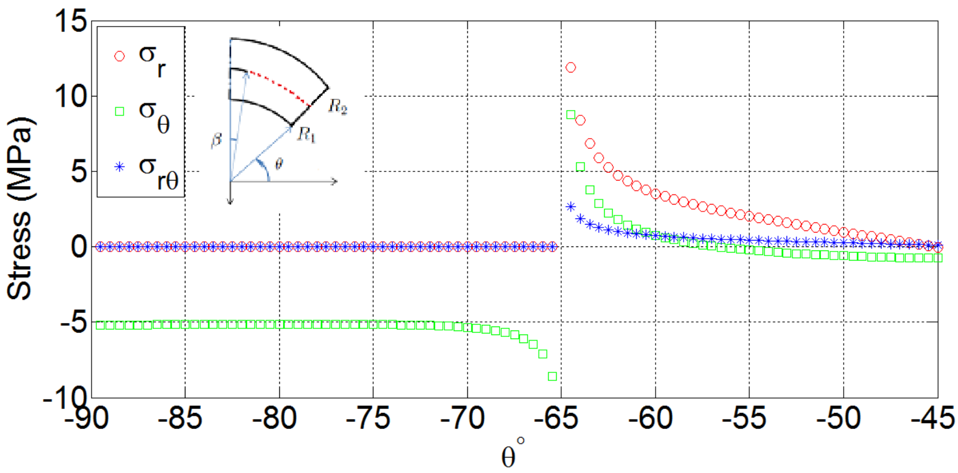

Figure 3.2: Stress variation on the arc that includes the crack for the *sample beam*

SIFs. In the subsections **3.1.1 - 3.1.3**, the calculations are carried out for a *sample beam* of $30mm$ in thickness ($R_1 = 15mm$ and $R_2 = 45mm$) containing a crack of 25° half arc angle, β, which is located on its center line ($R_a = 30mm$). In subsection **3.1.4** the effect of geometrical parameters variation on mode-I SIF and mode-mixity is studied.

3.1.1 Versus photoelastic caustics

The code-produced maximum shear stress contours for the *sample beam* are shown in Figure 3.1-(a). The asymmetric maximum shear stress contour shape around the crack tip signifies the mixity of fracture modes. Uniformly changing contours near the inner radius imitates the rainbow-shaped fringes predicted by the classical solution (in absence of the crack). In the lower quarter of the beam thickness, moving radially towards the beam bottom there is a regularly increasing trend in the stress values. The maximum shear stress contours obtained from photoelastic 4-point bending test of a plexiglass specimen of the same dimensions is shown in Figure 3.1-(b).

Considering manufacturing imperfections (especially at crack tips) and also noting deflection of the test specimen (which is not incorporated in the MMC-generated plot), a good agreement is observed between the analytic and experimental results in terms of the contour shapes. In Figure 3.2, the stress components in polar coordinates are shown on the arc that includes the crack for the same case. The plot indicates $1/\sqrt{r}$ linear-elastic singularity at the crack tip. The *traction-free* conditions on the crack surface ($\sigma_r = 0, \sigma_{r\theta} = 0$) are satisfied to an order of $10^{-6} Pa$ (or $10^{-12} MPa$).

3.1.2 Versus FEA

For the purpose of quantitative comparison, ANSYS Mechanical APDL, the commercial finite elements analysis software, is used to model and analyse the problem (Appendix E). The *stress intensity* (which is an ANSYYS jargon defined as $2 * \tau_{max}$ and should not be confused with stress intensity factor (SIF)) contours of the whole body are plotted and shown in Figure 3.3-(a) from FEA, and Figure 3.3-(b) from MATLAB code applying the MMC method. Note that deformation is shown in the Figure 3.3-(a) (so that one may realize the opened crack), but is not incorporated in Figure 3.3-(b), where the crack *seems to be* closed. However the fringes are from rather different colors, their values are specified the same. Although the contours are not identical, a reasonable consistency can be observed between them. For the near-tip stress fringe signature to become more clear, a zoomed view is presented in Figures 3.4-(a) and (b), again from FEA and the MMC method respectively. Comparing the crack tip caustics in Figure 3.4-(a) with that of photoelastic test (Figure 3.1-b) one may recognize an increasing incompatibility by approaching the very vicinity of the crack tip, however, the case is just the opposite for Figure 3.4-(b). In an immediate neighbourhood of the crack front a clearly analogous crack-tip signature is provided by the MMC method. Since the near tip stress values are to be used for SIF calculation in the next stage, they are of vital importance for insuring accuracy of the results. However the specimen imperfection (especially at the crack tip) should not be ignored, the test stands as a measure of *reality.*

3.1.3 Accuracy

In addition to *relative residual* value (i.e. `norm(b-A*x)/norm(b)`) resulted from solving the linear system of equations in a least-squares sense; the stress values on the boundaries also provide a measure for the degree of solution accuracy. It can be shown that when the system is restricted to include only local force boundary condition equations, the calculated stresses on the boundary are more consistent with that of input values (namely `b` matrix), as this leads to smaller relative residual values.

The *recalculated* stress values on the boundaries give a measure of the solution accuracy. In Figure 3.5 the obtained normal stress distribution on the moment-exerted boundary is plotted (by the markers) together with the classical (Golovin's) solution (the solid line) for the *sample*

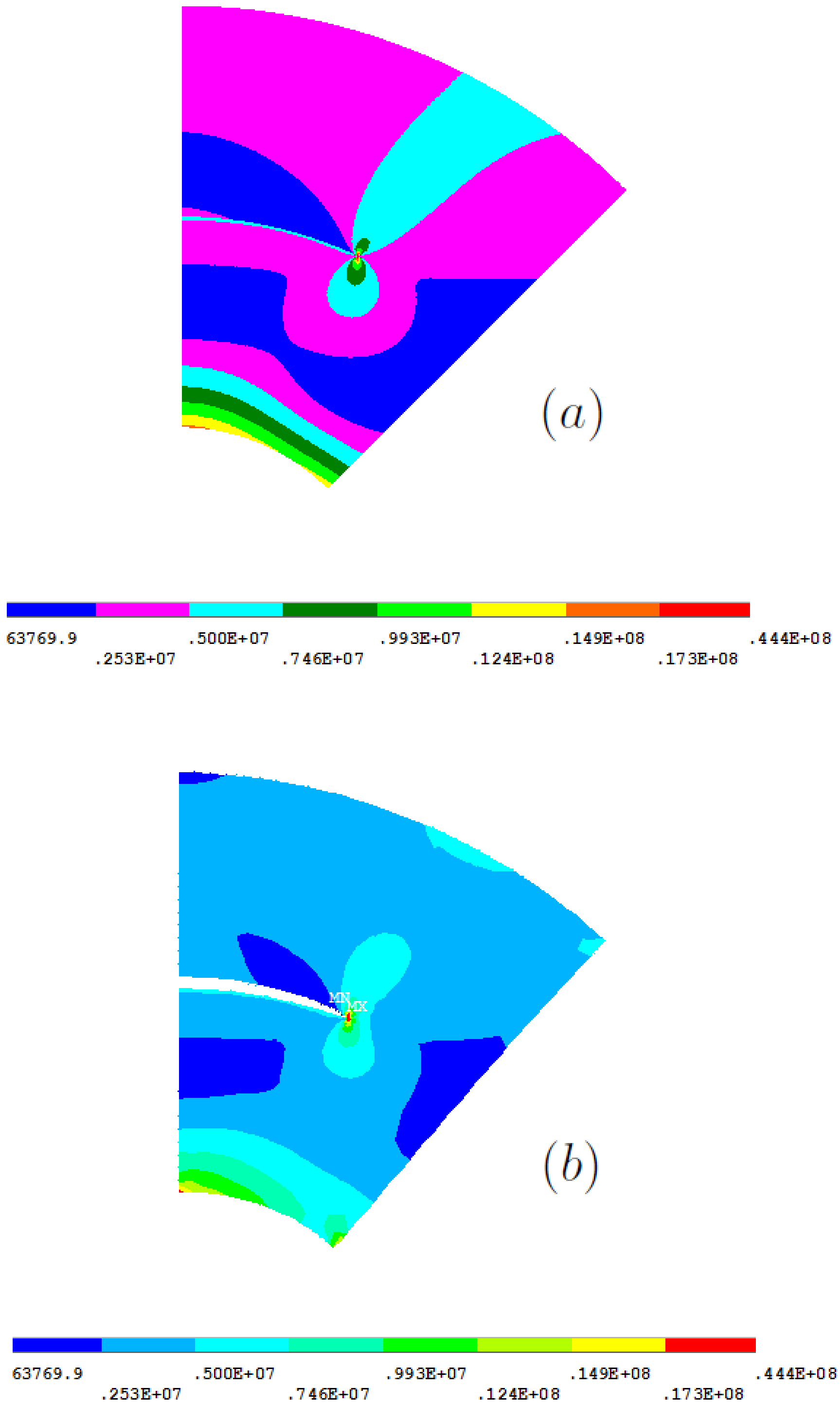

Figure 3.3: *Stress intensity* $(2 * \tau_{max})$ contours for the half sample beam containing a crack of $\beta = 25°$ at $h_a = 0.5$ obtained from (a) MATLAB code applying the MMC method and (b) ANSYS FEA

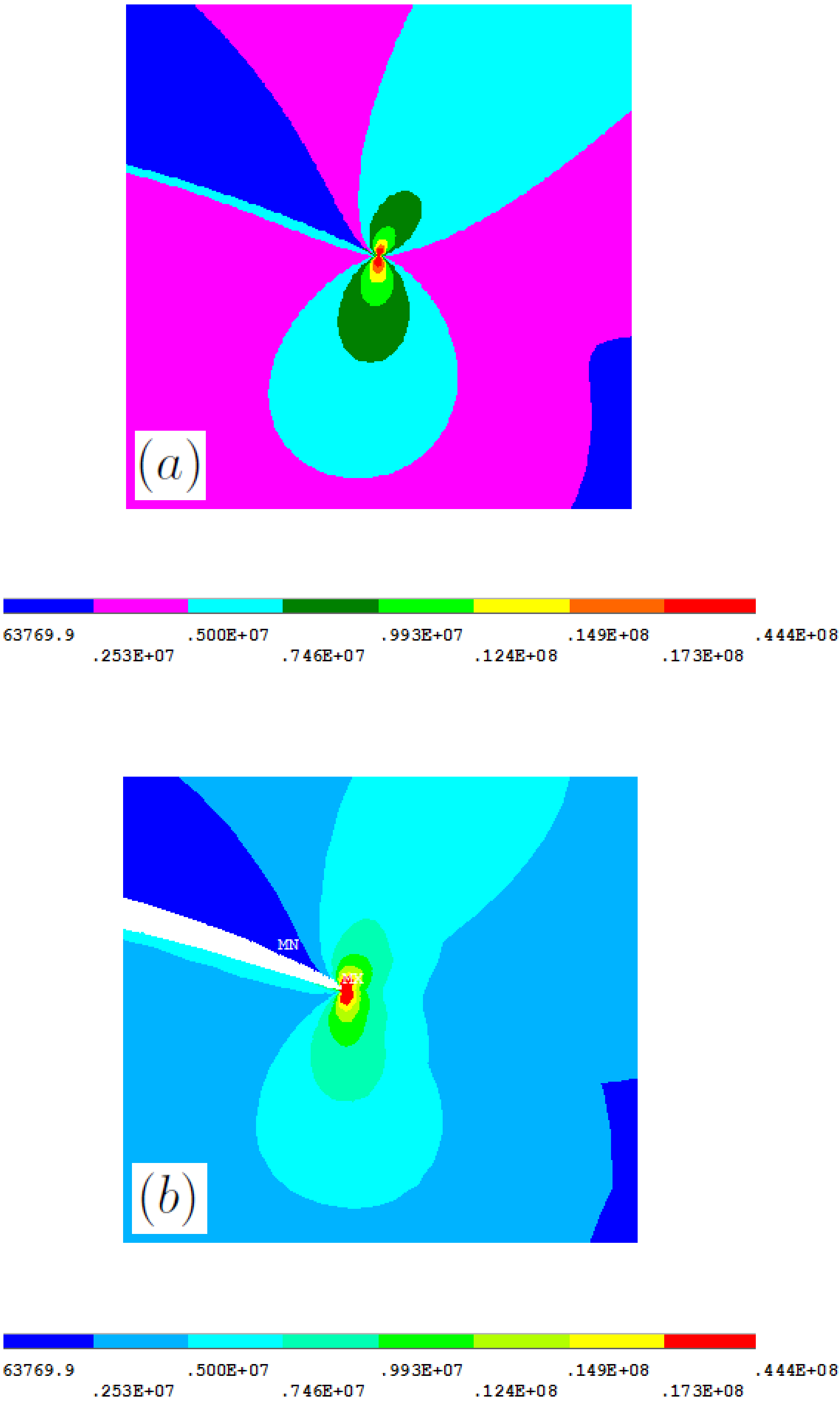

Figure 3.4: *Stress intensity* $(2 * \tau_{max})$ contours in 1 cm^2 vicinity of the crack-tip for the half sample beam containing a crack of $\beta = 25°$ at $h_a = 0.5$ obtained from (a) MATLAB code applying the MMC method and (b) ANSYS FEA

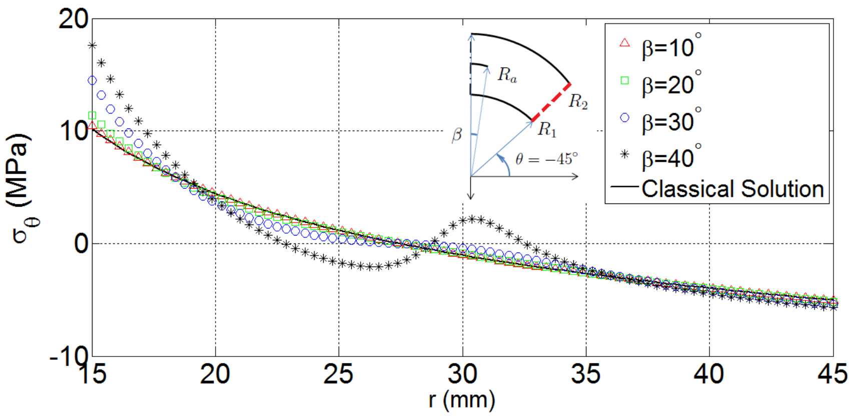

Figure 3.5: Deviation from the classical solution for normal stress distribution on the moment-exerted boundary for the *sample beam* with different β values

beam. Although the same distribution is expected, a deviation from the classical solution is observed with increase in the crack half arc angle (β). The *root mean square (RMS)* values of the deviation for β values $10°, 20°, 30°$ and $40°$ are calculated as $0.05, 0.25, 0.96$ and $2.19MPa$ respectively. Dividing by $\sigma = (\sigma_\theta)_{r=R_1} = 10.19MPa$, one has $0.5\%, 2.5\%, 9.4\%$ and 22% as a measure of the deviation from the classical solution. Also it is observed that all of the stress distributions, give nearly the same moment value about the origin (with a maximum of 3.2% deviation from $-10Nm$ for $\beta = 30°$, where for the other cases these values are below 0.5%). These distributions do not produce a *pure* moment; inducing a somewhat negligible non-zero force resultant in the circumferential direction. The fraction of these force values to the resultant of the positive σ_θ on the moment-exerted boundary reaches a maximum of 7.6% for $\beta = 40°$. The immediate neighbour is 1.36% for $\beta = 30°$. Generally, the smaller the cracks are the higher is the accuracy. On the other hand since initiating cracks are of prime concern loss of accuracy for handling large crack sizes is not of high importance practically. Obviously extrapolation could be done to some extent when needed.

Calculated value of the polar stress components, σ_r and $\sigma_{r\theta}$, ahead and in vicinity of crack-tip are of great importance for calculation of SIF values (see equations (2.32) and (2.33)). These values are extracted from both the MMC method and FEA on a segment of an arc to the center of xy plane, which includes the crack tip. In Figure 3.6, the MMC-resulted stress values are shown with markers whereas FEA-extracted stresses are plotted by solid lines. The FEA stress components first experience a jump at an angular position in $1°$ vicinity of the crack tip. Then, however σ_r results agree, the FEA $\sigma_{r\theta}$ values suddenly drop right before the crack-tip, while the MMC method-calculated values continue to increase according to the expectation of linear-elastic singularity at the crack-tip.

3.1.4 Parametric study

It is convenient to define a non-dimensionalized SIF parameter, H_i, as:

$$H_i = \frac{K_i}{\sigma\sqrt{2\pi R_m}} \tag{3.1}$$

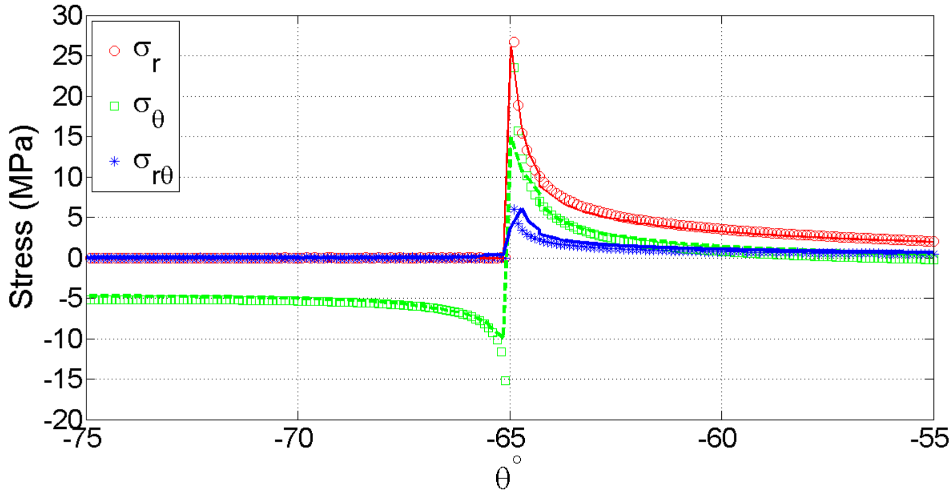

Figure 3.6: The markers represesnt the MMC method recalculated stresses in polar coordinates, the lines show the corresponding stress components extracted from ANSYS, both plotted for the points on a 20° arc with its center at the origin of the xy plane which has the crack tip at its midpoint and includes 10° of the crack surface

where σ is the value of the normal stress distribution in the classical (crack-less) solution at inner radius of the moment-exerted edge of the beam, R_m is the center line radius of the beam ($R_m = (R_1 + R_2)/2$); and i stands for either opening ($i \equiv I$) or sliding ($i \equiv II$) modes.

3.1.4.1 The crack position effect

The effect of the crack position along the thickness of the beam ($h_a = (R_a - R_1)/(R_2 - R_1)$) on mode-I SIF and the mode-mixity is shown in Figure 3.7 for a $30mm$ thick beam ($R_1 = 15mm, R_2 = 45mm$). Non-dimensional mode-I SIF, H_I, and mode-mixity, H_{II}/H_I, are plotted as a function of crack-half-arc-angle,β, in Figures 3.7-a and 3.7-b, respectively, for different crack positions $h_a = 0.25, 0.5$ and 0.75. For all crack positions, opening mode SIF is seen to increase rather linearly with crack size as seen in Figure 3.7-a. It is noted that the mode-I SIF is greater for crack positions closer to the inner radius. In Figure 3.7-b, the mode-mixity increases with crack size, however, its value remains always below unity, implying opening mode dominance (over sliding mode) for all of the $30mm$ thick beams. The mode-mixity is seen to be independent of crack position for smaller crack sizes, as indicated by the overlapping parts of the curves for $\beta < 15°$.

3.1.4.2 The beam thickness effect

The effect of thickness on the SIF and mode-mixity is shown in figure 3.8 for a central crack position kept fixed at $R_a = 30mm$. Non-dimensional opening mode SIF, H_I, (Figure 3.8-a) and mode-mixity, H_{II}/H_I, (Figure 3.8-b) are plotted against crack-half-arc-angle, β, for beam thicknesses $t = 10, 20$ and $30mm$. Since the same moment is applied to all of the cases, the narrower beams have higher SIF (K) values for their cracks (Figure 3.9). This is not evident

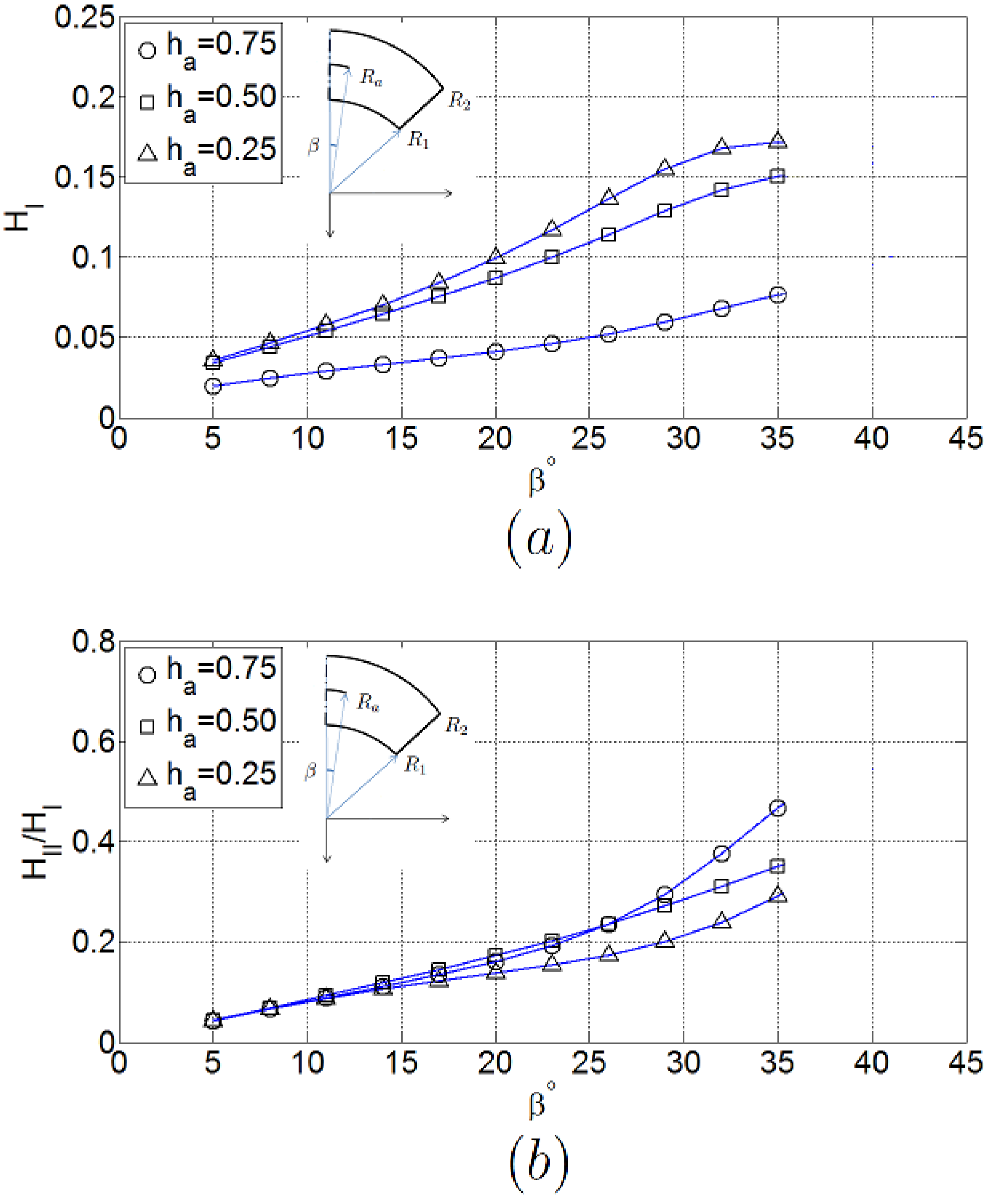

Figure 3.7: (a) Non-dimensionalized mode-I SIF and (b) Mode-mixity, versus crack half arc angle, β, for different crack positions $h_a = 0.25, 0.5$ and 0.75 for the beam with $R_1 = 15mm$ and $R_2 = 45mm$ for which the non-dimensionalising stress value is $\sigma = (\sigma_\theta)_{r=R_1} = 10.2MPa$

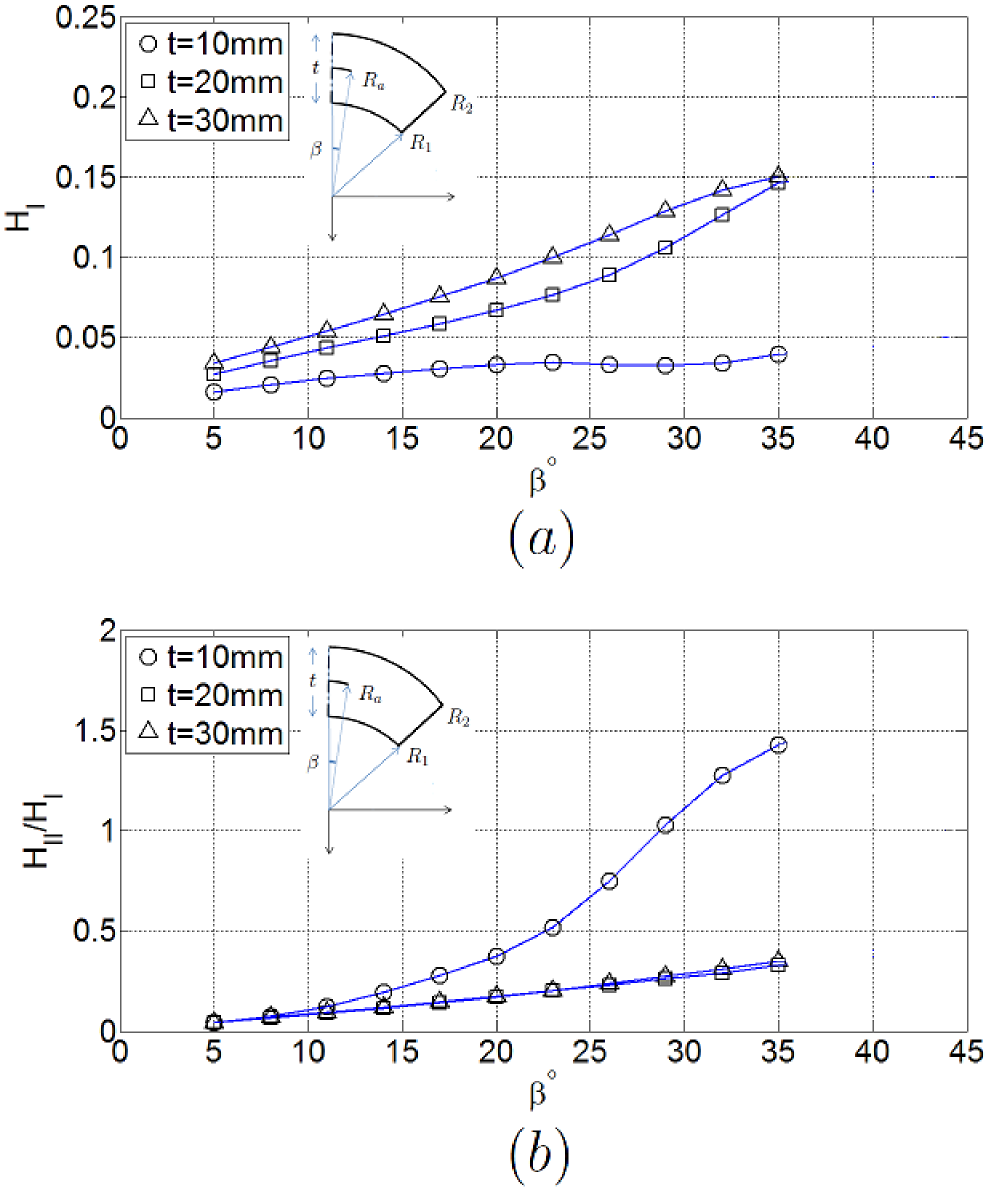

Figure 3.8: (a) Non-dimensionalized mode-I SIF and (b) Mode-mixity, versus crack half arc angle, β, for a central crack ($h_a = 0.5$) at $R_a = 30mm$, in beams of $t = 10, 20$ and $30mm$ thickness, for which corresponding non-dimensionalising stress values are $\sigma = (\sigma_\theta)_{r=R_1} = 67.6, 19.4$ and $10.2MPa$ respectively

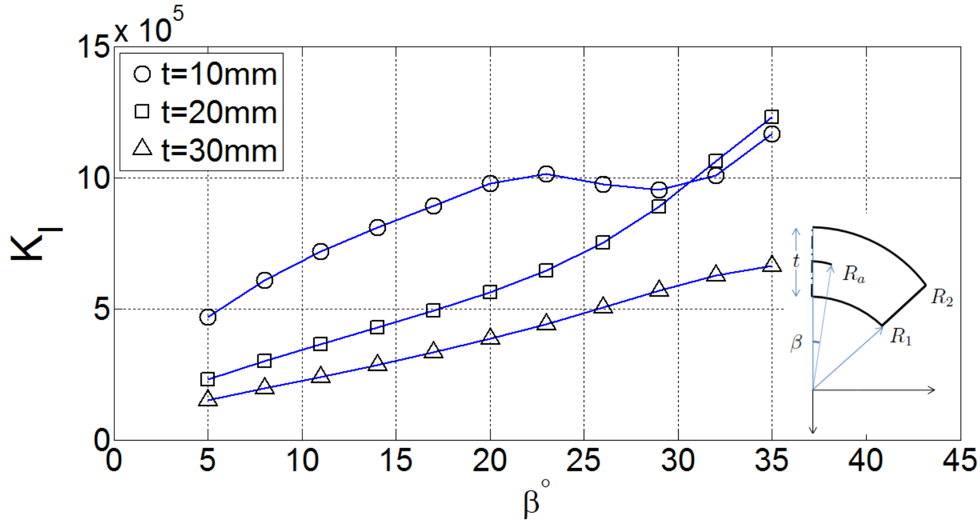

Figure 3.9: Mode-I SIF (K_I) versus crack half arc angle, β, for a central crack ($h_a = 0.5$) at $R_a = 30mm$ in beams of different thicknesses $t = 10,\ 20$ and $30mm$

from Figure 3.8-a because of non-dimensionalization done by equation (3.1); which involves the value of σ that varies inversely with beam thickness for a specified moment value. The σ values are given in the Figure caption. In Figure 3.8-a, the non-dimensional mode-I SIF increases monotonically with crack size for all thicknesses. The line slope for the beam of $10mm$ in thickness is relatively small. In Figure 3.8-b, mode-mixity increases with crack size for all thicknesses. At smaller crack sizes, mode-mixity remains below 0.1 for all thicknesses, showing an almost pure opening mode fracture. For the 20 and $30mm$ thick beams, the mode-mixity values almost overlap linearly increasing to a value of 0.35 at $\beta = 35°$. However, for the $10mm$ thick beam, the mode-mixity significantly deviates and following a non-linear trend reaches a value of 1.4 at $\beta = 35°$, rendering the crack tip mode-II dominated.

3.2 Conclusions

Using the stress correlation [3] technique, the stress field computed by the MMC method was successfully used to evaluate opening and sliding mode SIFs for a circumferential crack in an isotropic curved beam under pure bending. As a semi-analytic and *mesh-free* approach to treat boundary value problems of 2-D LEFM, the MMC method has a great advantage over other numerical methods such as finite elements, especially in dealing with the crack tip linear-elastic singularity, which makes it a proper choice for accurate calculation of SIF values.

The results of FEA using ANSYS Mechanical APDL shows a general compatibility with that of the MMC method in both qualitative and quantitative aspects. Compared with the FEA, the MMC method's near tip caustics appear to be more akin to that of photoelastic experiment.

The effects of crack position and beam thickness on the mode-I SIF and the mode-mixity are presented as a function of the crack size. As expected, the mode-I and mode-II SIFs increase with crack length. Considering different crack positions in the $30mm$ thick beam, the mode-I SIF values are found to be higher for the cracks closer to the inner radius. The mode-mixity is observed to be independent of the crack position and also to be below unity in all of the cases. Considering beams of different thicknesses ($10, 20$ and $30mm$), mode-I fracture is dominant in all cases except for the thinnest case in which a switch to the mode-II dominance happens for large crack lengths. The mode-mixity is found to be independent of the thickness for the thicker beams.

As a semi-analytic and mesh-free approach to treat boundary value problems of 2-D elasticity, the MMC method has a great advantage over other numerical methods such as finite elements, especially in dealing with the crack tip linear-elastic singularity, which makes it a proper choice for accurate calculation of SIF values. A possible subject of future work is to apply the method to analyze a circumferential crack in a cylindrically orthotropic curved beam.

REFERENCES

[1] Edwards T. and Thompson J., *Spar corner radius integrity for the A400M wing*, Applied Mechanics and Materials, vols. 3-4, pp. 197-202, (2005)

[2] ASTM D6415, *Standard test method for measuring the curved beam strength of a fiber-reinforced polymer-matrix composite*, American Society for Testing and Materials (ASTM) Standard (2006)

[3] Zehnder A. T., *Fracture mechanics*, Sibley School of Mechanical and Aerospace Engineering, Cornell University, (2010)

[4] Muskhelishvili N. I., *Some basic problems of the mathematical theory of elasticity*, P. Noordhoff, Groningen, (1953)

[5] Bowie O. L. and Neal D. M., *A modified mapping-collocation technique for accurate calculation of stress intensity factors*, International Journal of Fracture Mechanics, vol. 6, No. 2, pp. 199-206, (1970)

[6] Bowie O. L. and Freese C. E., *Central crack in plane orthotropic rectangular sheet*, International Journal of Fracture Mechanics, vol. 8, No. 1, pp. 49-58, (1972)

[7] Bowie O. L. and Freese C. E, *Elastic analysis for a radial crack in a circular ring*, Engineering Fracture Mechanics, vol. 4, pp. 315-321, (1972)

[8] Tracy P. G., *Analysis of a radial crack in a circular ring segment*, Engineering Fracture Mechanics, vol. 7, pp. 253-260, (1975)

[9] Tracy P. G., *Elastic analysis of radial cracks emanating from the outer and inner surfaces of a circular ring*, Engineering Fracture Mechanics, vol. 11, pp. 291-300, (1979)

[10] Timoshenko S. P. and Goodier J. N., *Theory of elasticity*, McGraw-Hill, New York, 3rd Edition, (1969)

[11] Guinea G. V., Planas J. and Elices M., *KI evaluation by the displacement extrapolation technique*, Engineering Fracture Mechanics, vol. 66, Issue 3, pp. 243-255, (2000)

[12] Jahed-motlagh H., Noban M. and Eshraghi M., *ANSYS Finite Elements* (in Farsi), University of Tehran Press, Tehran, 3rd Edition, (2006)

[13] Sokolnikoff I. S., *Mathematical theory of elasticity*, McGraw-Hill Book Company, New York, 2nd Edition, (1956)

[14] Wang C. T., *Applied elasticity*, McGraw-Hill Book Company, New York, (1953)

[15] Sih G. C., *Methods of analysis and solutions of crack problems: Recent developments in fracture mechanics theory and methods of solving crack problems (volume 1 of Mechanics of fracture)*, Noordhoff International Publications, Leyden, (1973)

[16] Palm III W. J., *Introduction to MATLAB 7 for engineers*, McGraw-Hill Book Company, New York, (2005)

[17] Hanselman D. and Littlefield B., *Mastering MATLAB 6: a comprehensive tutorial and reference*, Prentice Hall, Upper Saddle River, N.J., (2001)

[18] Attaway S., *MATLAB: A practical introduction to programming and problem solving*, Butterworth-Heinemann Ltd, Boston, (2009)

[19] McMohan D. M., *MATLAB demystified*, McGraw-Hill Book Company, New York, (2007)

[20] Higham D. J. and Higham N. J., *MATLAB guide*, Society for Industrial and Applied Mathematics (SIAM), Philadelphia, (2000)

[21] Griffiths D. F. and Higham D. J., *Learning LaTeX*, Society for Industrial and Applied Mathematics (SIAM), Philadelphia, (1997)

[22] Gratzer G., *First steps in LaTeX*, Birkhauser, Boston, (1999)

[23] `http://en.wikibooks.org/wiki/LaTeX`, *LaTeX wikibook*, 2011, (The latest browsing date by the thesis author is 26 February 2013, a PDF version is available for download)

[24] Oetiker T., Partl H., Hyna I. and Schlegl E., *The not so short introduction to LaTeX Or LaTeX in 157 minutes*, a free document, version 5.01, (2011)

[25] Oostrum P. V., *Page layout in LaTeX*, Department of Computer Science, Utrecht University, (2004)

[26] Krummel M., *LaTeX Tutorials*, `http://mrskrummel.com/tutorials`, 2009, (The latest browsing date by the thesis author is 26 February 2013)

APPENDIX A

MUSKHELISHVILI'S COMPLEX REPRESENTATIONS

Based on the general idea of developing a representation for the stress field that satisfies equilibrium and yields a single governing equation from the strain compatibility and strain-stress relations; the plane elasticity equations could be merged into the *biharmonic* equation:

$$\nabla^4 U = 0 \tag{A.1}$$

where the U function is called *Airy Stress Function* and $\nabla = \frac{\partial}{\partial x} + \frac{\partial}{\partial y}$. The above formula is the fundamental equation of the *boundary value problem* of two dimensional elasticity (for both *plane stress* and *plane strain* cases) on which the boundary condition equations are to be applied.

Starting from the equation (A.1), it will be shown that how did N. I. Muskhelishvili [4] use complex analysis tools to re-formulate the mentioned problem.

A.1 The stress function

Rewriting equation (A.1) as:

$$\nabla^2(\nabla^2 U) = 0 \tag{A.2}$$

Defining $\nabla^2 U = P(x, y)$:

$$\nabla^2 P = 0 \tag{A.3}$$

This means $P(x, y)$ satisfies the *Laplace* (or *harmonic*) equation. Defining the complex function $f(z)$ where $z = x + iy$ as:

$$f(z) = P(x, y) + iQ(x, y) \tag{A.4}$$

The real and imaginary parts of any *analytic function* of a complex variable are solutions of the Laplace equation. For $f(z)$ to be analytic in a region (i.e. to possess a unique derivative at any point of that region), the so-called *Cauchy-Reimann* conditions must hold:

$$\frac{\partial P}{\partial x} = \frac{\partial Q}{\partial y}, \quad \frac{\partial P}{\partial y} = -\frac{\partial Q}{\partial x} \tag{A.5}$$

Defining another complex function as:

$$\phi(z) = \frac{1}{4}\int f(z)dz = p(x, y) + iq(x, y) \tag{A.6}$$

Note that since $z = x + iy$, $\frac{\partial z}{\partial x} = 1$. According to the *chain rule*:

$$\frac{\partial}{\partial x}F(z) = \frac{d}{dz}F(z).\frac{\partial z}{\partial x} \tag{A.7}$$

so we conclude:

$$\frac{d}{dz} \equiv \frac{\partial}{\partial x} \tag{A.8}$$

considering (A.8), differentiating (A.6) with respect to z yields:

$$\phi'(z) = \frac{1}{4}(P + Q) = \frac{\partial p}{\partial x} + i\frac{\partial q}{\partial x} \tag{A.9}$$

equating the real and imaginary parts:

$$\frac{\partial p}{\partial x} = \frac{1}{4}P, \quad \frac{\partial q}{\partial x} = \frac{1}{4}Q \tag{A.10}$$

Considering Cauchy-Reimann conditions for $\phi(z)$:

$$\frac{\partial p}{\partial x} = \frac{\partial q}{\partial y}, \quad \frac{\partial p}{\partial y} = -\frac{\partial q}{\partial x} \tag{A.11}$$

Putting (A.10) and (A.11) together:

$$\frac{\partial p}{\partial x} = \frac{\partial q}{\partial y} = \frac{1}{4}P, \quad \frac{\partial q}{\partial x} = -\frac{\partial p}{\partial y} = \frac{1}{4}Q \tag{A.12}$$

On the other hand, applying the Laplace operator to the expression $xp + yq$:

$$\nabla^2(xp + yq) = (\frac{\partial^2}{\partial x^2} + \frac{\partial^2}{\partial y^2})(xp + yq)$$

$$\nabla^2(xp + yq) = 2\frac{\partial p}{\partial x} + 2\frac{\partial q}{\partial y} + x(\frac{\partial^2 p}{\partial x^2} + \frac{\partial^2 p}{\partial y^2}) + y(\frac{\partial^2 q}{\partial x^2} + \frac{\partial^2 q}{\partial y^2}) \tag{A.13}$$

Since p and q, as real and imaginary parts of the analytic function $\phi(z)$, satisfy the Laplace equation (i.e. $\nabla^2 p = \nabla^2 q = 0$):

$$\nabla^2(xp + yq) = 2\frac{\partial p}{\partial x} + 2\frac{\partial q}{\partial y} \tag{A.14}$$

substituting (A.1) into the above, leads to:

$$\nabla^2(xp + yq) = P \tag{A.15}$$

We had $\nabla^2 U = P$, eliminating P:

$$\nabla^2(U - xp - yq) = 0 \tag{A.16}$$

Defining $g(x, y) = U - xp - yq$, which satisfies the Laplace equation and therefore is a *harmonic* function, the stress function can be rewritten as:

$$U = xp + yq + g \tag{A.17}$$

Defining the analytic function $\chi(z) = g(x, y) + ih(x, y)$, and also noting:

$$\bar{z}\phi(z) = (xp + yq) + i(xq - yp) \tag{A.18}$$

one may write:

$$U = \Re\{\bar{z}\phi(z) + \chi(z)\} \tag{A.19}$$

or equally, eliminating the $\Re$ symbol:

$$U = \frac{1}{2}(\bar{z}\phi(z) + z\overline{\phi(z)} + \chi(z) + \overline{\chi(z)}) \tag{A.20}$$

A.2 Stress field equations

Note that since $z = x + iy$ and $\bar{z} = x - iy$, based on the chain rule:

$$\frac{\partial z}{\partial x} = 1 \;\Rightarrow\; \frac{\partial}{\partial x}F(z) = \frac{d}{dz}F(z)\frac{\partial z}{\partial x} \;\Rightarrow\; \frac{\partial}{\partial x} \equiv \frac{d}{dz} \tag{A.21}$$

$$\frac{\partial \bar{z}}{\partial x} = 1 \;\Rightarrow\; \frac{\partial}{\partial x}\overline{F(z)} = \frac{d}{d\bar{z}}\overline{F(z)}\frac{\partial \bar{z}}{\partial x} \;\Rightarrow\; \frac{\partial}{\partial x} \equiv \frac{d}{d\bar{z}} \tag{A.22}$$

$$\frac{\partial z}{\partial y} = i \;\Rightarrow\; \frac{\partial}{\partial y}F(z) = \frac{d}{dz}F(z)\frac{\partial z}{\partial y} \;\Rightarrow\; \frac{\partial}{\partial y} \equiv i\frac{d}{dz} \tag{A.23}$$

$$\frac{\partial \bar{z}}{\partial y} = -i \;\Rightarrow\; \frac{\partial}{\partial y}\overline{F(z)} = \frac{d}{d\bar{z}}\overline{F(z)}\frac{\partial \bar{z}}{\partial y} \;\Rightarrow\; \frac{\partial}{\partial y} \equiv -i\frac{d}{d\bar{z}} \tag{A.24}$$

Differentiating stress function (A.20) with respect to x (considering (A.21) and (A.22)):

$$\frac{\partial U}{\partial x} = \frac{1}{2}[\phi(z) + \bar{z}\phi'(z) + \overline{\phi(z)} + z\overline{\phi'(z)} + \chi'(z) + \overline{\chi'(z)}] \tag{A.25}$$

Similarly, considering (A.23) and (A.24):

$$i\frac{\partial U}{\partial y} = \frac{1}{2}[\phi(z) - \bar{z}\phi'(z) - \overline{\phi(z)} + z\overline{\phi'(z)} - \chi'(z) + \overline{\chi'(z)}] \tag{A.26}$$

summing up the last two equations:

$$\frac{\partial U}{\partial x} + i\frac{\partial U}{\partial y} = \phi(z) + \bar{z}\phi'(z) + \overline{\chi'(z)} \tag{A.27}$$

Defining $\psi(z) = \chi'(z)$:

$$\frac{\partial U}{\partial x} + i\frac{\partial U}{\partial y} = \phi(z) + z\overline{\phi'(z)} + \overline{\psi(z)} \tag{A.28}$$

The above relation will appear very useful in complex formulation of boundary condition equations beside providing a basis for stress field representation. Differentiating (A.28) with respect to x (again considering (A.21) and (A.22)):

$$\frac{\partial^2 U}{\partial x^2} + i\frac{\partial^2 U}{\partial x \partial y} = \phi'(z) + \overline{\phi'(z)} + z\overline{\phi''(z)} + \overline{\psi'(z)} \tag{A.29}$$

Differentiating (A.28) with respect to y (noting (A.23) and (A.24)), and multiplying both sides by $-i$:

$$\frac{\partial^2 U}{\partial y^2} - i\frac{\partial^2 U}{\partial x \partial y} = \phi'(z) + \overline{\phi'(z)} - z\overline{\phi''(z)} - \overline{\psi'(z)} \tag{A.30}$$

Adding (A.29) to (A.30):

$$\frac{\partial^2 U}{\partial^2 x} + \frac{\partial^2 U}{\partial^2 y} = 2(\phi'(z) + \overline{\phi'(z)}) \tag{A.31}$$

From elasticity, one may remember that Airy stress function was constructed basically as:

$$\sigma_x = \frac{\partial^2 U}{\partial y^2},\; \sigma_y = \frac{\partial^2 U}{\partial x^2},\; \sigma_{xy} = -\frac{\partial^2 U}{\partial x \partial y} \tag{A.32}$$

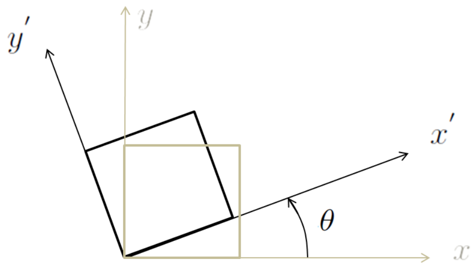

Figure A.1: The axes of element stress transformation

in order to satisfy the equilibrium equations automatically. Substituting the corresponding equations from above into (A.31):

$$\sigma_y + \sigma_x = 4\Re\{\phi'(z)\} \tag{A.33}$$

On the other hand, subtracting (A.30) from (A.29) and substituting from (A.32) into the yielded relation:

$$\sigma_y - \sigma_x - 2i\sigma_{xy} = 2[z\overline{\phi''(z)} + \overline{\psi'(z)}] \tag{A.34}$$

taking conjugate of both sides:

$$\sigma_y - \sigma_x + 2i\sigma_{xy} = 2[\bar{z}\phi''(z) + \psi'(z)] \tag{A.35}$$

The equations (A.33) and (A.35), formulated by G. V. Kolosov (as mentioned by N. I. Muskhelishvili [4]), show that stress field can be completely described in terms of two analytic functions $\phi(z)$ and $\psi(z)$. These equations may be called *Kolosov's stress field representation.*

A.3 Stress boundary condition equations

We are going to write stress on the boundaries in terms of its normal and tangential components. The *in-plane stress transformation* equations are:

$$\sigma_{x'} = \frac{1}{2}(\sigma_x + \sigma_y) + \frac{1}{2}(\sigma_x - \sigma_y)\cos(2\theta) + \sigma_{xy}\sin(2\theta) \tag{A.36}$$
$$\sigma_{y'} = \frac{1}{2}(\sigma_x + \sigma_y) - \frac{1}{2}(\sigma_x - \sigma_y)\cos(2\theta) - \sigma_{xy}\sin(2\theta) \tag{A.37}$$
$$\sigma_{x'y'} = \frac{1}{2}(\sigma_y - \sigma_x)\sin(2\theta) + \sigma_{xy}\cos(2\theta) \tag{A.38}$$

Adding (A.36) and (A.37):

$$\sigma_{x'} + \sigma_{y'} = \sigma_x + \sigma_y \tag{A.39}$$

On the other hand substituting (A.36),(A.37) and (A.38) into the expression $\sigma_{y'} - \sigma_{x'} + 2i\sigma_{x'y'}$, and re-factoring:

$$\begin{aligned}\sigma_{y'} - \sigma_{x'} + 2i\sigma_{x'y'} &= (\sigma_y - \sigma_x)[\cos(2\theta) + i\sin(2\theta)] \\ &\quad +2\sigma_{xy}[-\sin(2\theta) + i\cos(2\theta)]\end{aligned} \tag{A.40}$$

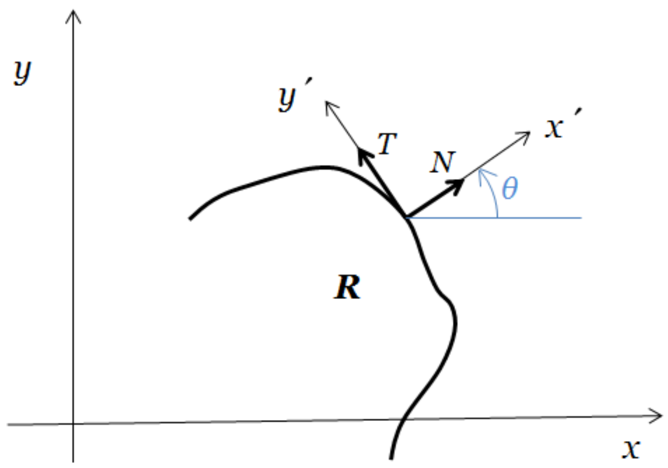

Figure A.2: The normal an tangential traction components on boundary of region "R"

Aside, the expression $-\sin(2\theta) + i\cos(2\theta)$ may be rewritten as:

$$-\sin(2\theta) + i\cos(2\theta) = \frac{1}{-i}[i\sin(2\theta) + \cos(2\theta)] \tag{A.41}$$

considering *Euler*'s Formula, $e^{i\alpha} = \cos(\alpha) + i\sin(\alpha)$:

$$-\sin(2\theta) + i\cos(2\theta) = ie^{2i\theta} \tag{A.42}$$

and therefore (multiplying both sides by $-i$):

$$\cos(2\theta) + i\sin(2\theta) = e^{2i\theta} \tag{A.43}$$

substituting (A.42) and (A.43) into (A.40):

$$\sigma_{y'} - \sigma_{x'} + 2i\sigma_{x'y'} = (\sigma_y - \sigma_x + 2i\sigma_{xy})e^{2i\theta} \tag{A.44}$$

which was stated for the first time by J. H. Michell.

Subtracting the sides of Michell's equation from those of (A.39), results in elimination of $\sigma_{y'}$:

$$2(\sigma_{x'} - i\sigma_{x'y'}) = \sigma_x + \sigma_y - (\sigma_y - \sigma_x + 2i\sigma_{xy})e^{2i\theta} \tag{A.45}$$

Note that the left hand side contains only normal and tangential stress components. One might rename them as $\sigma_{x'} \equiv N$ and $\sigma_{x'y'} \equiv T$. On the other hand making use of Kolosov's stress field representation (equations (A.33) and (A.35)); right hand side of (A.45) can be substituted. Then, the above formula may be rewritten as:

$$N - iT = \phi'(z) + \overline{\phi'(z)} - [\bar{z}\phi''(z) + \psi'(z)]e^{2i\theta} \tag{A.46}$$

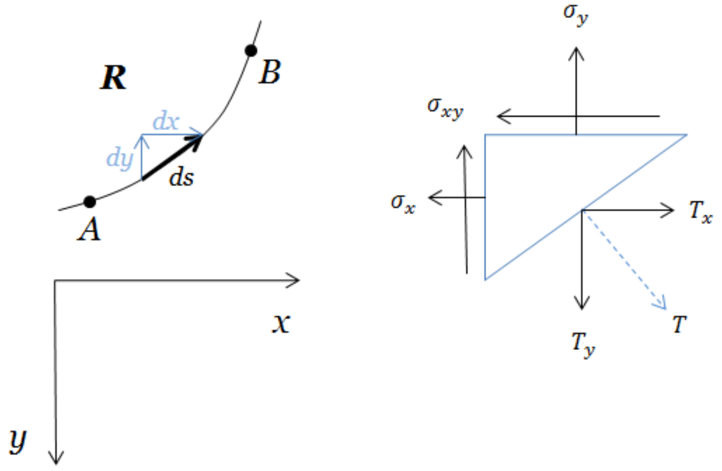

Figure A.3: Arc AB of the boundary of region "R" and corresponding infinitesimal element on it

A.4 Force boundary condition equations

Consider an element on an arc AB of boundary of the body "R" (Figure A.3). Let the arc's positive direction be from A to B. This means moving from A to B, we always have the body on the left, and then the normal vector to the right of the arc.

Writing force components equilibrium equation in x-direction:

$$T_x.ds - \sigma_x.|dy| - \sigma_{xy}.|dx| = 0 \tag{A.47}$$

consequently (noting that $dy < 0$):

$$T_x = \sigma_x(-\frac{dy}{ds}) + \sigma_{xy}(\frac{dx}{ds}) \tag{A.48}$$

substituting from (A.32):

$$T_x = -\frac{\partial^2 U}{\partial y^2}\frac{dy}{ds} - \frac{\partial^2 U}{\partial x \partial y}\frac{dx}{ds} \tag{A.49}$$

rewriting this way:

$$T_x = -[\frac{\partial}{\partial y}(\frac{\partial U}{\partial y})\frac{dy}{ds} + \frac{\partial}{\partial x}(\frac{\partial U}{\partial y})\frac{dx}{ds}] \tag{A.50}$$

The *total differential* is defined as:

$$\frac{df(x,y)}{dt} = \frac{\partial f}{\partial x}\frac{dx}{dt} + \frac{\partial f}{\partial y}\frac{dy}{dt} \tag{A.51}$$

considering $\frac{\partial U}{\partial y} \equiv f$; the equity (A.50) could be written briefly as:

$$T_x = -\frac{d}{ds}(\frac{\partial U}{\partial y}) \tag{A.52}$$

In a very similar manner, force components equilibrium equation in y-direction leads to:

$$T_y = \frac{d}{ds}(\frac{\partial U}{\partial x}) \tag{A.53}$$

Substituting the equations above into stress traction (i.e. $T = T_x + iT_y$), factoring out i:

$$T = i\frac{d}{ds}(\frac{\partial U}{\partial x} + i\frac{\partial U}{\partial y}) \tag{A.54}$$

replacing the expression in the parenthesis with that of equation (A.28):

$$T = i\frac{d}{ds}(\phi(z) + z\overline{\phi'(z)} + \overline{\psi(z)}) \tag{A.55}$$

or equally:

$$(T_x(s) + iT_y(s))ds = id(\phi(z) + z\overline{\phi'(z)} + \overline{\psi(z)}) \tag{A.56}$$

integrating the traction along AB, representing beam thickness in z-direction by b, one might express the force resultant components on arc AB as:

$$\begin{aligned}(F_x + iF_y)_{on\ arc\ AB} &= b.\int_A^B (T_x(s) + iT_y(s))ds \\ &= b.i[\phi(z) + z\overline{\phi'(z)} + \overline{\psi(z)}]_{z_A}^{z_B}\end{aligned} \tag{A.57}$$

A.5 Moment boundary condition equation

The moment resulted from the force components acting on the arc AB about the origin of the coordinate system xy, considering Figure A.3, is given by:

$$(M_z)_{on\ arc\ AB} = \int_A^B [-y.T_x(s) + x.T_y(s)]ds \tag{A.58}$$

substituting (A.52) and (A.53) into the above, one finds:

$$(M_z)_{on\ arc\ AB} = \int_A^B [y.d(\frac{\partial U}{\partial y}) + x.d(\frac{\partial U}{\partial x})] \tag{A.59}$$

implementing *integration by parts* on the first and second terms of the right hand side:

$$(M_z)_{on\ arc\ AB} = (x\frac{\partial U}{\partial x} + y\frac{\partial U}{\partial y})]_A^B - \int_A^B (\frac{\partial U}{\partial x}dx + \frac{\partial U}{\partial y}dy) \tag{A.60}$$

note that the integrand equals dU (i.e. is a total differential), thus:

$$(M_z)_{on\ arc\ AB} = (x\frac{\partial U}{\partial x} + y\frac{\partial U}{\partial y})]_A^B - [U]_A^B \tag{A.61}$$

aside, one finds:

$$x\frac{\partial U}{\partial x} + y\frac{\partial U}{\partial y} = \Re\{z(\frac{\partial U}{\partial x} - i\frac{\partial U}{\partial y})\} \tag{A.62}$$

further, taking conjugate of (A.28):

$$\frac{\partial U}{\partial x} - i\frac{\partial U}{\partial y} = \overline{\phi(z)} + \bar{z}\phi'(z) + \psi(z) \tag{A.63}$$

substituting (A.63) into (A.62):

$$x\frac{\partial U}{\partial x} + y\frac{\partial U}{\partial y} = \Re\{z\overline{\phi(z)} + z\bar{z}\phi'(z) + z\psi(z)\} \tag{A.64}$$

On the other hand, the equation (A.19) may be written as:

$$U = \Re\{z\overline{\phi(z)} + \chi(z)\} \tag{A.65}$$

Putting (A.64) and (A.65) into right hand side. (A.61):

$$(M_z)_{on\ arc\ AB} = \Re\{[z\bar{z}\phi'(z) + z\psi(z) - \chi(z)]_{z_A}^{z_B}\} \tag{A.66}$$

where, since we defined previously $\chi'(z) = \psi(z)$:

$$\chi(z) = \int \psi(z)dz \tag{A.67}$$

APPENDIX B

CONFORMAL MAPPING AND ITS AIM

Why do we use *conformal mapping*? What is the advantage held by transferring the physical domain into the *image plane*?

The mapping performed by an *analytic function* $h(\zeta)$ is called *conformal.* By means of $z = h(\zeta)$, an analytic function of complex variable z becomes another analytic function of the complex variable ζ. However, the boundary curve of the domain $\mathbf{R}$ in the z-plane, which may not be convenient to work with, could be treated in the ζ-plane that allows the boundary condition to be satisfied more easily. The advantages of mapping become more apparent especially when there is a crack in the body under investigation.

B.1 The mapping function

The problem of circumferential crack, due to its geometry, needs two successive mappings. Combining these functions relates the ζ-plane (in which the problem is solved) to the z-plane (to which the solution will be transferred back). The *composite mapping function* $z = h(\zeta)$ allows rewriting z-plane formulations in terms of ζ. In fact, the mapping is performed from the ζ-plane to the z-plane, because the intended image is already there and the formulae should be *mapped* to. After the solution process done, the results may be transferred back into the physical plane again.

The first function maps the unit circle (and its exterior) in the ζ-plane into the straight crack (and its exterior) in w-plane:

$$w = g(\zeta) = \frac{L}{4}(\zeta + \zeta^{-1}) \tag{B.1}$$

where L is the length of the straight crack in the w-plane. It can be shown how does this happen by substituting $\zeta = e^{i\theta} = \cos(\theta) + i\sin(\theta)$ (i.e. unit circle equation) into the above formula, which yields $w = \frac{L}{2}\cos(\theta)$.

The second function maps the straight crack (and its exterior) resulted in the w-plane, into the circumferential crack (and its exterior) in the z-plane:

$$z = f(w) = R_a \exp\{i(w - \frac{\pi}{2})\} \tag{B.2}$$

where R_a is crack radius in z-plane. Solving the above for z, considering $z = z(r_z, \theta_z)$:

$$w = (\theta_z + \frac{\pi}{2}) - i\ln(\frac{r_z}{R_a}) \tag{B.3}$$

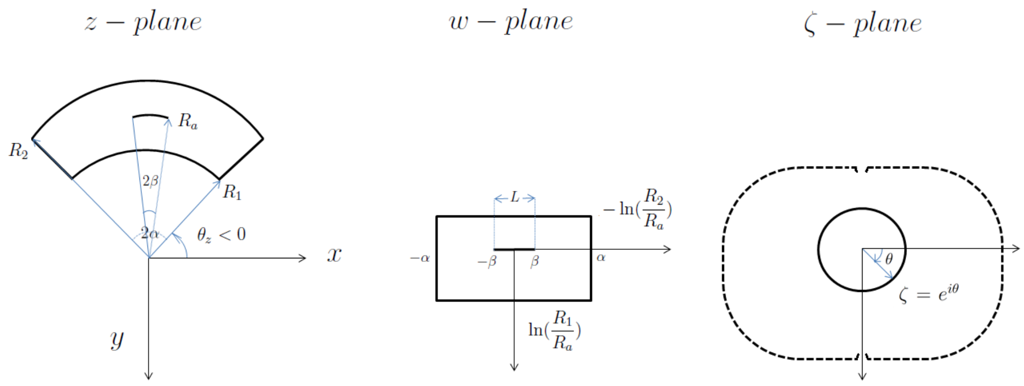

Figure B.1: The successive mapping plan

by which it can be shown that $L = 2\beta$. Then (B.1) can be rewritten as:

$$w = g(\zeta) = \frac{\beta}{2}(\zeta + \zeta^{-1}) \tag{B.4}$$

Therefore, combining the first and second mappings one finds the *composite* function which maps the unit circle ($|\zeta| = 1$) and its exterior into the circumferential crack and the curved beam (as its exterior) as:

$$z = f(g(\zeta)) = h(\zeta) = R_a \exp\{i[\frac{\beta}{2}(\zeta + \zeta^{-1}) - \frac{\pi}{2}]\} \tag{B.5}$$

The $h(\zeta)$ function enables transferring analytic functions in z-plane to those in ζ-plane.

On the other hand, solving (B.4) for ζ yields:

$$\zeta = \frac{w \pm \sqrt{w^2 - \beta^2}}{\beta} \tag{B.6}$$

Substituting (B.3) into the above, ζ can be obtained as a function of z. The equation (B.6) declares that the relation between ζ and w planes has a dual feature. It can be shown (maybe using MATLAB plotting functions) that if the plus sign is selected, *only the right half* of the rectangle in the w-plane (see Figure B.1) is mapped exterior to the unit circle (and to the right hand side of the imaginary axis) in the ζ-plane, while the *left half* of the rectangle is mapped into the unit circle. Besides, by choosing the minus sign, *only left half* of the rectangle is mapped exterior to the unit circle and to left hand side of the imaginary axis while the right half of the rectangle is mapped into the unit circle. This is why in Figures B.1 and C.1 the mapped boundary in the ζ-plane is divided into right and left parts.

B.2 Kartzivadze's continuation argument

In close relation to application of conformal mapping to the *cracked body* problems, the concept of *analytic continuation* developed by I. N. Kartzivadze (for the unit circle) and later by N. I. Muskhelishvili (for the real axis).

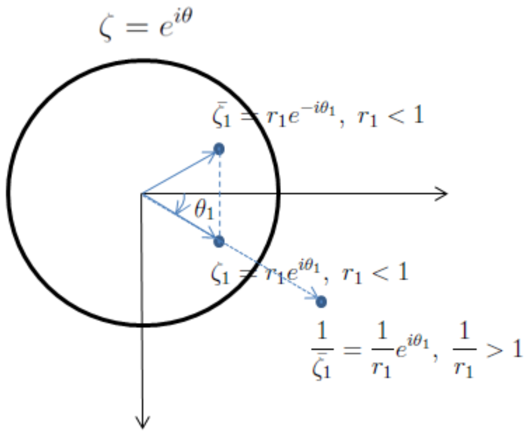

Figure B.2: The unit circle interior, and exterior

Let the function $\phi(\zeta)$ (in the image plane), to be *extended* into the interior unit circle (i.e. inside the crack image) by defining:

$$\phi(\zeta) = -\frac{h(\zeta)}{\overline{h'}(\frac{1}{\zeta})}\overline{\phi'}(\frac{1}{\zeta}) - \overline{\psi}(\frac{1}{\zeta}), \qquad for\ |\zeta| < 1 \tag{B.7}$$

where:

$$\overline{fn}(\frac{1}{\zeta}) = \overline{fn(\frac{1}{\overline{\zeta}})} \tag{B.8}$$

The equation (B.7) is called *Kartzivadze's continuation (or extension) argument* as it causes the $\phi(\zeta)$ function *continue* across into the unit circle.

Taking *conjugate* from (B.7), and reordering:

$$\overline{\overline{\psi}(\frac{1}{\zeta})} = -\overline{\phi(\zeta)} - \frac{\overline{h(\zeta)}}{\overline{\overline{h'}(\frac{1}{\zeta})}}\overline{\overline{\phi'}(\frac{1}{\zeta})}, \qquad for\ |\zeta| < 1 \tag{B.9}$$

noting that according to (B.8),

$$\overline{\overline{fn}(\frac{1}{\zeta})} = fn(\frac{1}{\overline{\zeta}}) \tag{B.10}$$

one has:

$$\psi(\frac{1}{\overline{\zeta}}) = -\overline{\phi}(\overline{\zeta}) - \frac{\overline{h}(\overline{\zeta})}{h'(\frac{1}{\overline{\zeta}})}\phi'(\frac{1}{\overline{\zeta}}), \qquad for\ |\zeta| < 1 \tag{B.11}$$

changing the notation by putting:

$$\frac{1}{\overline{\zeta}} \to \zeta_* \Longrightarrow \overline{\zeta} \to \frac{1}{\zeta_*} \tag{B.12}$$

note that if ζ is inside unit circle (i.e. $|\zeta| < 1$), which is so for the equation (B.11), then $\frac{1}{\overline{\zeta}} \equiv \zeta_*$ is outside unit circle (see Figure(B.2)). Therefore:

$$\psi(\zeta) = -\overline{\phi}(\frac{1}{\zeta}) - \frac{\overline{h}(\frac{1}{\zeta})}{h'(\zeta)}\phi'(\zeta), \qquad for\ |\zeta| > 1 \tag{B.13}$$

Note that $|\zeta| > 1$ means for every point on the body. This result is of extreme importance from two aspects; firstly expressing $\psi(\zeta)$ in terms of $\phi(\zeta)$, reduces number of analytic functions needed to describe the *Airy stress function* to one (i.e. solely $\phi(\zeta)$); and secondly it analytically makes *traction-free* conditions on the crack surfaces satisfied by keeping left hand side of the force boundary conditions zero on the unit circle which renders the equations automatically satisfied (see section 2.2).

APPENDIX C

THE LAURENT SERIES REPRESENTATION

What is the proper series expansion for the $\phi(\zeta)$ function? How does *stress symmetry* with respect to the *imaginary axis* affect that expansion?

C.1 The Laurent series

According to the *Laurent theorem*, for any function (e.g. $\phi(\zeta)$) that is analytic on an *annulus* **R**, centred at $\zeta = 0$, there exists a *unique* power series expansion of the form:

$$\phi(\zeta) = \sum_{n=-\infty}^{+\infty} a_n \zeta^n \tag{C.1}$$

which converges to that function on the region **R**, namely a *Laurent Series*.

Although in the case of cracked curved beam, the outer mapped boundary is not circular; there is no a priori reason to suspect that the region of convergence of the series could not be extended over to a it. Hence, it seems possible to approximate the $\phi(\zeta)$ by a *truncated* Laurent series there.

C.2 The effect of stress symmetry

Stress symmetry with respect to the imaginary axis requires the stress field on the left-half of the body to *mirror* that of the right-half. This means that normal stresses (σ_x and σ_y) at $-\bar{\zeta}$ must be respectively equal to those at ζ. Also, with shear stress τ at ζ, there must be $-\tau$ at $-\bar{\zeta}$ (see Figure (C.1)). We are going to see how the above requisition may affect the series expansion form of $\phi(\zeta)$. In other words, we want to investigate the possibility of taking into account the stress symmetry of the problem as an innate property of the series expansion such that it could automatically satisfy the boundary conditions on the axis of symmetry.

Consider Kolosov's stress field representation (Appendix A) in the image plane:

$$\sigma_y + \sigma_x = 4\Re\{\frac{\phi^{'}(\zeta)}{h^{'}(\zeta)}\} \tag{C.2}$$

$$\sigma_y - \sigma_x + 2i\tau = 2\{\overline{h(\zeta)}\,\frac{h^{'}(\zeta)\phi^{''}(\zeta) - h^{''}(\zeta)\phi^{'}(\zeta)}{[h^{'}(\zeta)]^2} + \psi^{'}(\zeta)\}/h^{'}(\zeta) \tag{C.3}$$

According to Kartzivadze's extension argument (Appendix B, section B.2) the $\psi(\zeta)$ function expressed in terms of $\phi(\zeta)$ by equation B.13, differentiating with respect to ζ yields:

$$\psi^{'}(\zeta) = -\overline{\phi}'(\frac{1}{\zeta}) + [\frac{\overline{h}(\frac{1}{\zeta})\cdot h^{''}(\zeta)}{[h^{'}(\zeta)]^2} - \frac{\overline{h}^{'}(\frac{1}{\zeta})}{h^{'}(\zeta)}]\cdot\phi^{'}(\zeta) - \frac{\overline{h}(\frac{1}{\zeta})}{h^{'}(\zeta)}\cdot\phi^{''}(\zeta) \tag{C.4}$$

Name *right hand side* of equation(C.3) as Ω. Substituting the above relation into Ω and reordering:

$$\Omega(\zeta) = 2\{[\frac{h^{''}(\zeta)}{[h^{'}(\zeta)]^3}\cdot(\overline{h}(\frac{1}{\zeta}) - \overline{h(\zeta)}) - \frac{\overline{h}^{'}(\frac{1}{\zeta})}{[h^{'}(\zeta)]^2}]\cdot\phi^{'}(\zeta) + \frac{\overline{h(\zeta)} - \overline{h}(\frac{1}{\zeta})}{[h^{'}(\zeta)]^2}\cdot\phi^{''}(\zeta) - \frac{\overline{\phi}^{'}(\frac{1}{\zeta})}{h^{'}(\zeta)}\} \tag{C.5}$$

Name the complex coefficients of $\phi^{'}(\zeta)$ and $\phi^{''}(\zeta)$ in the above relation as $\omega_1(\zeta)$ and $\omega_2(\zeta)$ respectively. It may be shown that:

$$\Re\{\omega_1(\zeta)\} = \Re\{\omega_1(-\overline{\zeta})\} \tag{C.6}$$

$$\Im\{\omega_1(\zeta)\} = -\Im\{\omega_1(-\overline{\zeta})\} \tag{C.7}$$

$$\Re\{\omega_2(\zeta)\} = -\Re\{\omega_2(-\overline{\zeta})\} \tag{C.8}$$

$$\Im\{\omega_2(\zeta)\} = \Im\{\omega_2(-\overline{\zeta})\} \tag{C.9}$$

Also:

$$\Re\{h^{'}(\zeta)\} = \Re\{h^{'}(-\overline{\zeta})\} \tag{C.10}$$

$$\Im\{h^{'}(\zeta)\} = -\Im\{h^{'}(-\overline{\zeta})\} \tag{C.11}$$

In the light of these relations, considering equations (C.2) and (C.3) the conditions for stress symmetry can be formulated as given below:

For $\sigma_x(\zeta) = \sigma_x(-\overline{\zeta})$ and $\sigma_y(\zeta) = \sigma_y(-\overline{\zeta})$ to be held:

$$\Re\{\frac{\phi^{'}(\zeta)}{h^{'}(\zeta)}\} = \Re\{\frac{\phi^{'}(-\overline{\zeta})}{h^{'}(-\overline{\zeta})}\} \tag{C.12}$$

which considering equation (C.10), may be reduced to:

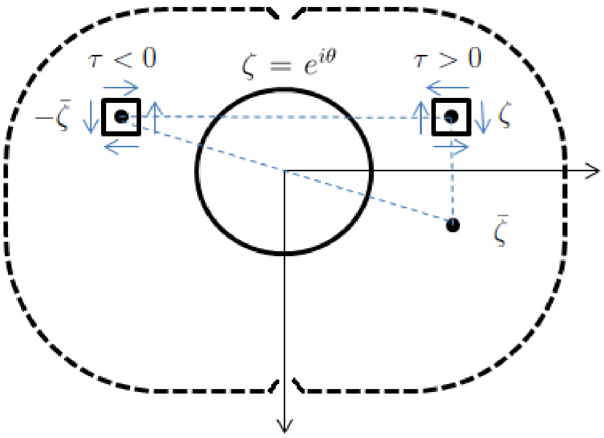

Figure C.1: The *punctured region*'s symmetry and mirrored shear stress

$$\Re\{\phi^{'}(\zeta)\} = \Re\{\phi^{'}(-\bar{\zeta})\} \tag{C.13}$$

also, noting the equation (C.3):

$$\Re\{\Omega(\zeta)\} = \Re\{\Omega(-\bar{\zeta})\} \tag{C.14}$$

On the other hand, considering equation (C.3), to keep $\tau(\zeta) = -\tau(-\bar{\zeta})$, it is necessary to have:

$$\Im\{\Omega(\zeta)\} = -\Im\{\Omega(-\bar{\zeta})\} \tag{C.15}$$

Thus for stress symmetry conditions to become satisfied by the form of $\phi(\zeta)$ function series expansion, there exist three requirements; namely equations (C.13), (C.14) and (C.15).

Rewriting series expansion (C.1) by separating even and odd exponents of ζ:

$$\phi(\zeta) = \sum_{n=-\infty}^{+\infty} [a_{2n}\zeta^{2n} + a_{2n+1}\zeta^{2n+1}] \tag{C.16}$$

one has:

$$\phi^{'}(\zeta) = \sum_{n=-\infty}^{+\infty} [2n.a_{2n}\zeta^{2n-1} + (2n+1)a_{2n+1}\zeta^{2n}] \tag{C.17}$$

$$\phi^{'}(-\bar{\zeta}) = \sum_{n=-\infty}^{+\infty} [-2n.a_{2n}\bar{\zeta}^{2n-1} + (2n+1)a_{2n+1}\bar{\zeta}^{2n}] \tag{C.18}$$

also:

$$\phi^{''}(\zeta) = \sum_{n=-\infty}^{+\infty} [2n(2n-1)a_{2n}\zeta^{2n-2} + 2n(2n+1)a_{2n+1}\zeta^{2n-1}] \tag{C.19}$$

$$\phi^{''}(-\bar{\zeta}) = \sum_{n=-\infty}^{+\infty} [2n(2n-1)a_{2n}\bar{\zeta}^{2n-2} - 2n(2n+1)a_{2n+1}\bar{\zeta}^{2n-1}] \tag{C.20}$$

The first requirement for the stress symmetry was equation (C.13), which can be written as:

$$\Re\{\phi^{'}(\zeta) - \phi^{'}(-\bar{\zeta})\} = 0 \tag{C.21}$$

substituting C.17 and C.18 into the above equation:

$$\Re\{\sum_{n=-\infty}^{+\infty} [2n.a_{2n}(\zeta^{2n-1} + \bar{\zeta}^{2n-1}) + (2n+1)a_{2n+1}(\zeta^{2n} - \bar{\zeta}^{2n})]\} = 0 \tag{C.22}$$

since $\zeta^{2n-1} + \bar{\zeta}^{2n-1}$ is always a *purely real* expression, and $\zeta^{2n} - \bar{\zeta}^{2n}$ is *purely imaginary*; for the above equation to be satisfied for every ζ, a_{2n} is to be purely imaginary and a_{2n+1} must be purely real. Mathematically, the notation is changed as:

$$a_{2n} \equiv iA_{2n} \tag{C.23}$$

$$a_{2n+1} \equiv A_{2n+1} \tag{C.24}$$

where A_{2n} and A_{2n+1} are *purely real* coefficients of the series expansion.

On the other hand, for the second requirement (equation (C.14)) to be true, there are three sub-requirements:

$$\Re\{\phi^{'}(\zeta)\} = \Re\{\phi^{'}(-\bar{\zeta})\} \tag{C.25}$$

$$\Re\{\phi^{''}(\zeta)\} = -\Re\{\phi^{''}(-\bar{\zeta})\} \tag{C.26}$$

$$\Re\{\overline{\phi}'(\frac{1}{\zeta})\} = \Re\{\overline{\phi}'(-\frac{1}{\bar{\zeta}})\} \tag{C.27}$$

The first one is the same as equation (C.13), and therefore is previously satisfied.

Substituting (C.19) and (C.20) into (C.26) leads to:

$$\Re\{\sum_{n=-\infty}^{+\infty} [2n(2n-1)a_{2n}\overbrace{(\zeta^{2n-2} + \bar{\zeta}^{2n-2})}^{purely\ real} + 2n(2n+1)a_{2n+1}\overbrace{(\zeta^{2n-1} - \bar{\zeta}^{2n-1})}^{purely\ imaginary}]\} = 0 \tag{C.28}$$

which is again satisfied by considering (C.23) and (C.24).

Before expanding sides of (C.27), note that according to the definition ($\overline{fn}(\zeta) = \overline{fn(\overline{\zeta})}$):

$$\overline{\phi}'(\frac{1}{\zeta}) = \overline{\phi'(\frac{1}{\overline{\zeta}})} \tag{C.29}$$

and similarly:

$$\overline{\phi}'(-\frac{1}{\overline{\zeta}}) = \overline{\phi'(-\frac{1}{\overline{\overline{\zeta}}})} = \overline{\phi'(-\frac{1}{\zeta})} \tag{C.30}$$

substituting (C.29) and (C.30) into (C.27):

$$\Re\{\overline{\phi'(\frac{1}{\overline{\zeta}})}\} = \Re\{\overline{\phi'(-\frac{1}{\zeta})}\} \tag{C.31}$$

taking conjugate from the sides of (C.31):

$$\Re\{\phi'(\frac{1}{\overline{\zeta}})\} = \Re\{\phi'(-\frac{1}{\zeta})\} \tag{C.32}$$

Now expanding the sides of (C.32) according to (C.17) and reordering:

$$\Re\{\sum_{n=-\infty}^{+\infty} [2n.a_{2n} \overbrace{(\overline{\zeta}^{1-2n} + \zeta^{1-2n})}^{purely\ real} + (2n+1)a_{2n+1} \overbrace{(\overline{\zeta}^{-2n} - \zeta^{-2n})}^{purely\ imaginary}]\} = 0 \tag{C.33}$$

this equation is also satisfied by setting (C.23) and (C.24). Thus, up to now it is shown that $\sigma_x(\zeta) = \sigma_x(-\overline{\zeta})$ and $\sigma_y(\zeta) = \sigma_y(-\overline{\zeta})$ is guaranteed.

Finally; equation (C.15) is investigated. It needs a little more carefulness, since the habitual principles of algebra may mislead the analysis with complex variables.

First consider the term $\omega_1(\zeta).\phi^{'}(\zeta)$ in C.5. Noting equations (C.6), (C.7) and (C.13); for the imaginary part of this term to change sign by converting ζ to $-\overline{\zeta}$:

$$\Im\{\phi^{'}(\zeta)\} = -\Im\{\phi^{'}(-\overline{\zeta})\} \tag{C.34}$$

must be held. Now consider the term $\omega_2(\zeta).\phi^{''}(\zeta)$; noting equations (C.8), (C.9) and (C.25), for its imaginary part to change sign at symmetrical points with respect to the imaginary axis:

$$\Im\{\phi^{''}(\zeta)\} = \Im\{\phi^{''}(-\overline{\zeta})\} \tag{C.35}$$

is a must. Lastly, for the term $\overline{\phi'(\frac{1}{\zeta})}/h^{'}(\zeta)$, considering (C.10), (C.11) and (C.27):

$$\Im\{\overline{\phi}'(\frac{1}{\zeta})\} = -\Im\{\overline{\phi}'(-\frac{1}{\overline{\overline{\zeta}}})\} \tag{C.36}$$

therefore the third requirement is broken into three sub-requirements; namely equations (C.34), (C.35) and (C.36).

Expanding (C.34), by using (C.17) and (C.18):

$$\Im\{\sum_{n=-\infty}^{+\infty}[2n.a_{2n}\overbrace{(\zeta^{2n-1}-\overline{\zeta}^{2n-1})}^{purely\ imaginary}+(2n+1)a_{2n+1}\overbrace{(\zeta^{2n}+\overline{\zeta}^{2n})}^{purely\ real}]\}=0 \tag{C.37}$$

Expanding (C.35), by using (C.19) and (C.20):

$$\Im\{\sum_{n=-\infty}^{+\infty}[2n(2n-1)a_{2n}\overbrace{(\zeta^{2n-2}-\overline{\zeta}^{2n-2})}^{purely\ imaginary}+2n(2n+1)a_{2n+1}\overbrace{(\zeta^{2n-1}+\overline{\zeta}^{2n-1})}^{purely\ real}]\}=0 \tag{C.38}$$

On the other hand, substituting (C.29) and (C.30) into (C.36):

$$\Im\{\overline{\phi'(\frac{1}{\overline{\zeta}})}\} = -\Im\{\overline{\phi'(-\frac{1}{\overline{\overline{\zeta}}})}\} \tag{C.39}$$

taking conjugate:

$$\Im\{\phi'(\frac{1}{\overline{\zeta}})\} = -\Im\{\phi'(-\frac{1}{\zeta})\} \tag{C.40}$$

Expanding (C.40), making use of (C.17) and (C.18):

$$\Im\{\sum_{n=-\infty}^{+\infty}[2n.\overline{a_{2n}}\overbrace{(\overline{\zeta}^{-2n-1}-\zeta^{-2n-1})}^{purely\ imaginary}-(2n+1)\overline{a_{2n+1}}\overbrace{(\zeta^{-2n-2}+\overline{\zeta}^{-2n-2})}^{purely\ real}]\}=0 \tag{C.41}$$

It is obvious that $a_{2n}\equiv iA_{2n}$ and $a_{2n+1}\equiv A_{2n+1}$ do also satisfy the sub-requirements (C.37), (C.38) and (C.41).

All of the three general conditions (C.13), (C.14) and (C.15) for the *stress symmetry with respect to the imaginary axis* are shown to be held by the arguments (C.23) and (C.24). Since a truncation of the Laurent series is to be used, (C.1) can be rewritten as:

$$\phi(\zeta) = \sum_{n=-M}^{N}[iA_{2n}\zeta^{2n}+A_{2n+1}\zeta^{2n+1}] \tag{C.42}$$

where M and N are non-negative integers and A_{2n} and A_{2n+1} are *purely real.* The *mirror characteristic* of the stress components with respect to the imaginary axis is built-into the $\phi(\zeta)$ function series expansion form.

APPENDIX D

PURE BENDING OF A CURVED BEAM

In some problems of plane elasticity in the polar coordinates, the stress distribution is obviously the same in all radial cross sections. Considering these θ*-independent* cases, one may find [10] that the biharmonic equation in its polar form can be reduced to an ordinary differential equation, which its general solution is of the form:

$$U = A\ln(r) + Br^2\ln(r) + Cr^2 + D \tag{D.1}$$

where U is the Airy stress function and A,B,C and D are constants of integration and are to be determined from the boundary conditions.

D.1 The equivalent stress distribution

The problem of curved beam under pure bending is one of those cases which is natural to expect stress θ-independence. Applying the boundary conditions (noting that the force equilibrium condition is satisfied automatically by the chosen form of (D.1)):

$$\sigma_r(r) = 0, \qquad (for\ r = R_1\ and\ r = R_2) \tag{D.2}$$

$$b\int_{R_1}^{R_2} r\sigma_\theta(r)dr = -M \tag{D.3}$$

$$\sigma_{r\theta}(r) = 0, \qquad (on\ whole\ boundary) \tag{D.4}$$

to (A.32) equations in their polar form, A,B,C and D, and thereby U are obtained [10]; then one has:

$$\sigma_r(r) = -\frac{4M}{N_G b}[\frac{R_1^2R_2^2}{r^2}\ln(\frac{R_2}{R_1}) + R_2^2\ln(\frac{r}{R_2}) + R_1^2\ln(\frac{R_1}{r})] \tag{D.5}$$

$$\sigma_\theta(r) = -\frac{4M}{N_G b}[-\frac{R_1^2R_2^2}{r^2}\ln(\frac{R_2}{R_1}) + R_2^2\ln(\frac{r}{R_2}) + R_1^2\ln(\frac{R_1}{r}) + R_2^2 - R_1^2] \tag{D.6}$$

$$\sigma_{r\theta}(r) = 0 \tag{D.7}$$

where:

$$N_G = (R_2^2 - R_1^2)^2 - 4R_1^2R_2^2(\ln(\frac{R_2}{R_1}))^2 \tag{D.8}$$

and b stands for depth in z-direction. This solution is due to H. Golovin. A normal stress distribution as of (D.6) at the ends of the beam produces a pure bending *couple* $-M$.

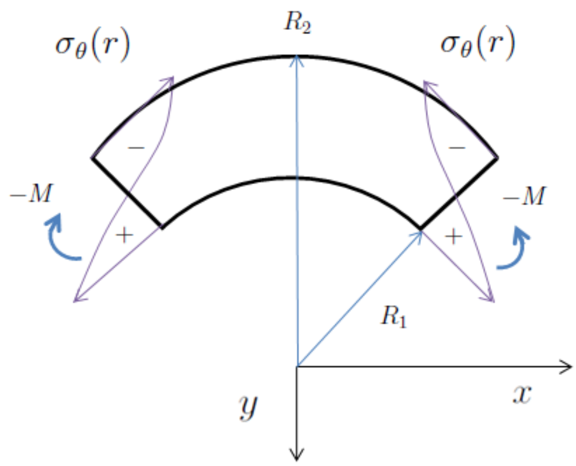

Figure D.1: The opening couple and its equivalent stress distribution on the boundary

D.2 Force resultants

Knowing the stress distribution at the ends of the beam, it becomes possible to obtain force resultant vector acting on any arbitrary segment there:

$$(F_x + iF_y)_{on\ \overline{AB}} = b. \int_A^B [T_x(s) + iT_y(s)]ds \tag{D.9}$$

where $T_x(s)$ and $T_y(s)$ are stress traction vector components and s represents surface of the boundary, which in the present case coincides with the polar coordinate r.

Considering Figure (D.2):

$$T_x(s) = -\sigma_\theta(r). \sin(-\frac{\pi}{2} + \alpha) \tag{D.10}$$

$$T_y(s) = \sigma_\theta(r). \cos(-\frac{\pi}{2} + \alpha) \tag{D.11}$$

where α is half-arc angle of the beam and here equals $pi/4$ (note that $-\pi/2 + \alpha$ is a negative value). Substituting these into (D.9):

$$(F_x + iF_y)_{on\ \overline{AB}} = b.[-\sin(\alpha - \frac{\pi}{2}) + i\cos(\alpha - \frac{\pi}{2})]. \int_A^B \sigma_\theta(r)dr \tag{D.12}$$

Aside, substituting *Golovin*'s solution (D.6), and integrating:

$$\int_A^B \sigma_\theta(r)dr = -\frac{4M}{N_G b}[R_1^2 r \ln(\frac{R_1}{r}) + R_2^2 r \ln(\frac{r}{R_2}) + \frac{R_1^2 R_2^2}{r} \ln(\frac{R_2}{R_1})]_{r_A}^{r_B} \tag{D.13}$$

substituting this into the previous, b is eliminated:

$$(F_x + iF_y)_{on\ \overline{AB}} = -[\cos(\alpha) + i\sin(\alpha)]. \\ \frac{4M}{N_G}[R_1^2 r \ln(\frac{R_1}{r}) + R_2^2 r \ln(\frac{r}{R_2}) + \frac{R_1^2 R_2^2}{r} \ln(\frac{R_2}{R_1})]_{r_A}^{r_B} \tag{D.14}$$

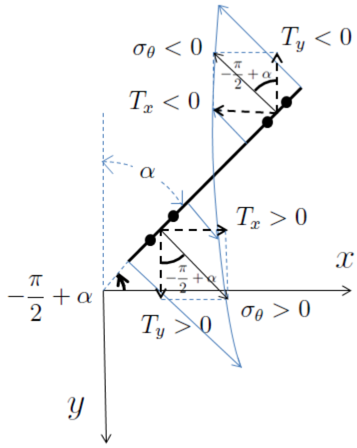

Figure D.2: The stress traction vector on the moment-exerted end of the beam

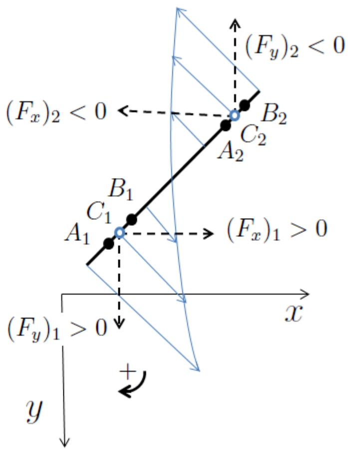

Figure D.3: The force components on the moment-exerted end of the beam

where M is the absolute value of the exerted couple and N_G is given by (D.8).

Considering the bell shape form of the expression $R_1^2 r \ln(\frac{R_1}{r}) + R_2^2 r \ln(\frac{r}{R_2}) + \frac{R_1^2 R_2^2}{r} \ln(\frac{R_2}{R_1})$ (when plotted with respect to r), and comparing this with Figure (D.2) reveals the requirement of $r_B > r_A$ namely the necessity of *moving in the positive direction* when one makes use of (D.14); which otherwise needs to be multiplied by -1 to produce force values with compatible sign.

D.3 Moments

Finally we come by the moment produced on a segment $\overline{AB}$ of the beam end (Figure (D.3)):

$$(M_z)_{on\ \overline{AB}} = |x_c|.F_y + |y_c|.F_x \tag{D.15}$$

where $|x_c|$ and $|y_c|$ are absolute values of moment arms about the origin. Obviously F_x and F_y obtained in the previous section (by equation(D.14)) can be used again. Putting the force components with their sign into the above relation, it may be checked that the formula produces moment values compatible with the up to now applied sign convention.

APPENDIX E

ANSYS PROCEDURES

In order to evaluate the MMC method solution, the problem of *a circumferential crack in an isotropic curved beam under pure bending* modelled and analysed by ANSYS release 14.0 Mechanical APDL (from which *ANSYS Workbench* is descended). A finite element model is developed for the crack arc half angle, β, equal to 25°. The crack is positioned at the middle of the beam thickness ($h_a = 0.5$). The beam inner and outer radii are $R_1 = 15mm$ and $R_2 = 45mm$ respectively. The results are given and discussed in chapter 3. This appendix plans to describe the procedures followed to come up with the results of the EFA. To begin modelling, two primary steps are to be taken: determining the element type and inputting the mechanical properties.

The recommended element type by ANSYS documentation for a 2-D fracture model is PLANE183, the 8-node quadratic solid. The specified element type will be used for meshing. Considering the dimensions of the beam, a plane state of stress is assumed. The plexiglass (PMMA) mechanical properties are given to the software although these are not going to affect the results of the *stress* analysis according to the theory of elasticity.

The first step in the *preprocess*ing stage is to specify the element type:

`ANSYS Main Menu>Preprocessor>Element Type>Add/Edit/Delete`

in the *Element Types* dialog box push the *Add* button. In the *Library of element types* dialog box, in the left hand side list select *Solid* and then on the right hand side select *8 node 183*. The *PLANE 183* element type is defined in the *Element Types* dialog box. Push the *Options* button. In the opening dialog box for *Element Shape* choose *Quadrilateral*, for *Element behavior* select *Plane strs w/thk* (i.e. plane state of stress assumption with specifying thickness) and for *Element formulation* let the *Pure displacement* remain. Push *Ok* and *Close* buttons.

Now the beam thickness in z-direction (which contrary to ANSYS jargon is named here as *width* of the beam) can be specified without necessarily making a 3-D model:

`ANSYS Main Menu>Preprocessor>Real Constants>Add/Edit/Delete`

in the *Real Constants* dialog box push the *Add* button. In the *Element type for real constant* dialog box push the *Ok* button. In the opening dialog box set *THK* (thickness) to $0.01m$. Push the *Ok* and *Close* buttons.

The second step is to input the mechanical properties of the model. One may enter the mechanical properties of plexiglass (PMMA) as $EX = 2.4E + 009Pa$ for Young modulus and

$PRXY = 0.28$ for Poisson ratio in the dialog box appearing by:

`ANSYS Main Menu>Preprocessor>Material Props>Material Models`

and selecting *Structural*, *Linear*, *Elastic* and *Isotropic*.

E.1 Modelling

To model the crack, it is not acceptable to use a notch or wedge at the crack tip. Rather, the discontinuity is to be ended by a sudden integration of the crack surfaces. In Figure E.1 the model constructed for the half-beam is shown. For the case under study, making the crack requires the *Area*s (i.e `A1`, `A2`, `A3` and `A4` in Figure E.1) to be *Glued* at all their common boundaries other than where the crack is planned to exist. Specifying the geometry starts with determining the *Keypoint*s, note that two overlying keypoints should be specified on the intersection of the crack *surfaces* and the "imaginary"axis:

`ANSYS Main Menu>Preprocessor>Modelling>Create>Keypoints>In Active CS`

then creating the *Arcs*, note that two overlying arcs should be specified as the surfaces of the crack. They start from two distinct (but overlying) keypoints which lay on the symmetry axis and end at the same keypoint at the crack tip. The procedure for each arc is:

`ANSYS Main Menu>Preprocessor>Modelling>Create>Lines>Arcs>By End KPs & Rad`

select both of the two keypoints from which the arc passes, click apply button, select the arc-center keypoint (which is the origin of the coordinate system), and then click apply again. In the dialog box enter the arc radius.

The straight lines can be specified by:

`ANSYS Main Menu>Preprocessor>Modelling>Create> Lines>Lines>In Active Coord`

Then, selecting the corresponding lines the areas can be specified by:

`ANSYS Main Menu>Preprocessor>Modelling>Create> Areas>Arbitrary>By Lines`

and the final stage of modeling is the *gluing* procedure for the areas:

`ANSYS Main Menu>Preprocessor>Modelling>Operate> Booleans>Glue>Areas`

note that the areas `A1` and `A2` (Figure E.1) are not to be glued (as the final part of the trick planned to model the crack).

E.2 Meshing

One of the ways by which user can change the automatic mesh produced by ANSYS (possibly for the purpose of generating a finer mesh) is to determine the number of divisions on the lines constructing the modelled body:

`ANSYS Main Menu>Preprocessor>Meshing>Meshtool`

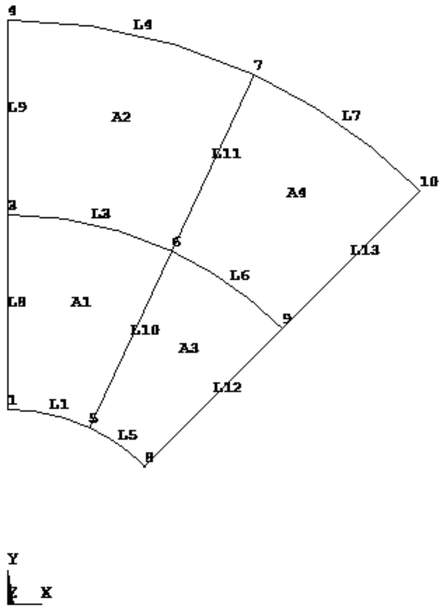

Figure E.1: The half-beam ANSYS *model*

then from *Size Controls* section, push the *set* button for *Lines*. By determining number of divisions (*NDIV*) the element nodes can be placed in equal distances from each other. It is specially helpful when the loading is to be applied as a force distribution on the nodes. In the case study, NDIV is set to 8 for `L1` and `L5` (Figure E.1) and to 16 for the others.

The crack tip meshing should be considered carefully. According to ANSYS Help, quadratic quarter-point (singular) elements are to be used. It automatically generates two rows of these elements around the crack tip by commanding:

`ANSYS Main Menu>Preprocessor>Meshing>Size Cntrls>Concentrat KPs>Create`

and choosing the crack tip keypoint. In the dialog box, *DELR* determines the radius of the first (inner) row of the singular elements around the crack tip (it was set to $0.1mm$). According to the Help it should be smaller than the length of the crack divided by eight. *RRAT* is the ratio of the difference between radii of outer and inner rows of the singular elements to the radius of the inner row of the elements around the crack tip (it was set to 0.5, which means that the radius of the outer element row is 3/2 times bigger than the inner). *NTHET* specifies the number of singular elements in each 90° around the crack tip in the circumferential direction. Again according to the Help, roughly one element every 30° or 40° is recommended. This means that *NTHET* should not be more than three(it was set to 3). Finally *KCTIP* has two options. Due to the tutorial, quarter point ($1/4pt$) skewed element should be selected, for which the midside nodes are placed at the quarter points. After entering the values push the apply button and then the *Mesh* button on the *Mesh tool* dialog box for mesh to be generated.

Node No.	F_x	F_y	Node No.	F_x	F_y
1	58.27	-58.27	17	-9.06	9.06
2	50.22	-50.22	18	-11.20	11.20
3	43.15	-43.15	19	-13.24	13.24
4	36.88	-36.88	20	-15.18	15.18
5	31.27	-31.27	21	-17.03	17.03
6	26.21	-26.21	22	-18.81	18.81
7	21.62	-21.62	23	-20.51	20.51
8	17.42	-17.42	24	-22.14	22.14
9	13.58	-13.58	25	-23.71	23.71
10	10.02	-10.02	26	-25.22	25.22
11	6.73	-6.73	27	-26.68	26.68
12	3.67	-3.67	28	-28.09	28.09
13	0.80	0.80	29	-29.45	29.45
14	-1.89	1.89	30	-30.77	30.77
15	-4.41	4.41	31	-32.04	32.04
16	-6.80	6.80			

TableE.1: The force components applied to the nodes (in Newtons)

E.3 Applying the boundary conditions

Taking advantage of the stress symmetry, half of the beam is modelled. This requires zero horizontal displacement for the nodes on the axis of symmetry:

`ANSYS Main Menu>Solution>Define Loads>Apply>Structural>Displacement>`
`(Symmetry B.C.)>On Nodes`

In addition, to prevent the rigid body motion (which causes trivial solutions), the lowest node on the symmetry boundary is to be fixed in the vertical direction (Figure E.2).

To apply loading in terms of forces on the nodes of the moment-exerted boundary, command:

`ANSYS Main Menu>Solution>Define Loads>Apply>Structural>Force/Moment>On Nodes`

The force vector components are given in the table E.1. The moment-exerted boundary is divided to 32 equal segments and therefore includes 65 (corner and midside) nodes (Figure E.2). Although there is no ban on force application on the midside nodes, the force components are applied to the 31 corner nodes, starting from the corner node immediately above R_1 (namely node number 1 in the table) and ending at the corner node right before R_2. These values are obtained from multiplying σ_θ distribution given by Golovin (Appendix D) into the area of the boundary division on which it acts (and is equal to $b * (R_2 - R_1)/16$, where b is the beam width). Applying point forces on the nodes at the corners avoided.

A simpler way to apply the the moment to the curved part of the beam requires modelling of the whole L-shaped beam as in the Figures 1.1 or 1.3 (in the later ignore the *bonded surface*). Then to produce pure bending moment for the curved section of the beam it becomes possible

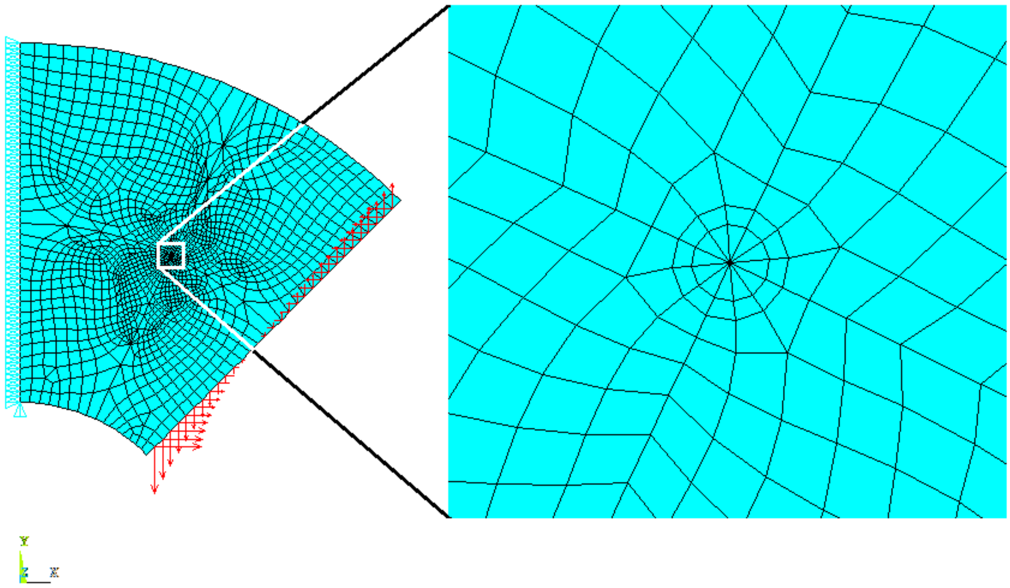

Figure E.2: The boundary conditions applied on the body and a close view of the crack-tip vicinity mesh, where two rows of singular elements are generated

to apply two uniform *pressure* (stress) distributions on the lines `L17` and `L24` (Figure E.3). Since the *handle* of the beam is divided to four parts of $50mm$ in length and considering that the beam width is $0.1mm$, the value of the pressure to produce a $10Nm$ moment can be calculated as $0.2MPa$. This modelling strategy not only eliminates the need for node by node application of the force components but also provides a more accurate boundary condition definition in terms of loading. By commanding:

```
ANSYS Main Menu>Solution>Define Loads>Apply>Structural>Pressure>On Lines
```

picking the lines and pressing *Ok* button, the pressure value can be inserted to the opening dialog box.

E.4 Solving and plotting

After meshing the model and applying the boundary conditions the problem is ready to be solved by:

```
ANSYS Main Menu>Solution>Solve>Current LS
```

After the solution is done, a range of plotting options for stress field becomes available, among which exists *Stress Intensity* (it may not be confused with the stress intensity factor, SIF). ANSYS documentation defines *Stress Intensity* as $2 * \tau_{max}$. Thus do not concern if the *maximum shear* expression does not appear in the lengthy list of options. After commanding:

```
ANSYS Main Menu>General Postproc>Plot Results>Contour Plot>Nodal Solu
```

in the *Contour Nodal Solution Data* dialog box, click the *Stress* folder and then the *Stress*

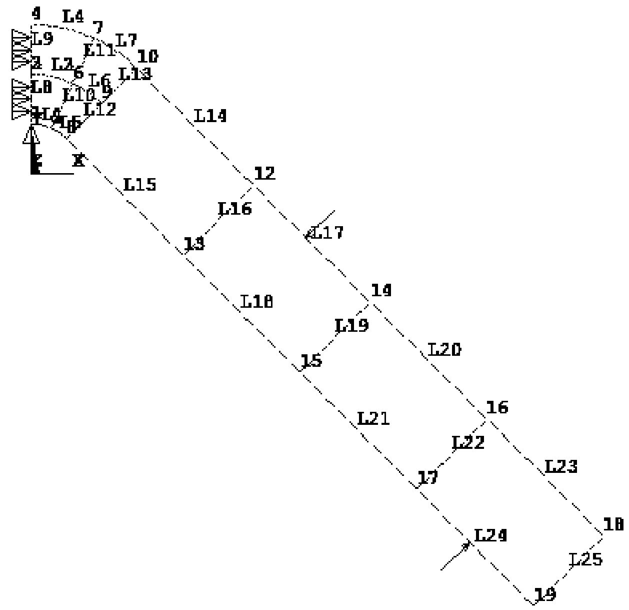

Figure E.3: An alternative finite element modelling strategy

intensity and push the *Ok* button.

E.5 Reading and listing the stress values

To read the stress component values at a specified point in the Cartesian coordinates, command:

`ANSYS Main Menu>General Postproc>Query Results>Subgrid Solu`

In the *Query Subgrid Solution Data* dialog box choose *Stress* from the left hand side list and select `SX`, `SY` or `SXY` to read σ_x, σ_y and σ_{xy}. Note that also the node coordinates can be red from the picking (*Query Subgrid Results*) pallet. ANSYS only allows reading the stress values at the element corners (and not on the midside nodes).

On the other hand, to list the stress component values of a certain set of nodes, firstly it is required to define a *path* by commanding:

`ANSYS Main Menu>General Postproc>Path Operations>Define Path>By Nodes`

then to specify the path by selecting the nodes. The path may be named arbitrarily. The next step is to determine the parameters that you want to be extracted into the list:

`ANSYS Main Menu>General Postproc>Map onto Path`

in the opening dialog box, from the left hand side menu select stress and from the right hand side menu, choose `SX`, `SY` and `SXY` (which are ANSYS symbols for σ_x, σ_y and σ_{xy}) by pressing *Apply* button each time. Finally, command:

```
ANSYS Main Menu>General Postproc>List Results>Path Items
```

in the openin window, select the path name and the *items* `XG`, `YG`, `SX`, `SY` and `SXY` from the menus. Push the *Ok* button to produce the list.

In order to export the list to MATLAB, first the list may be copied and pasted into an Excel sheet. The reason is that the list should be prepared as a matrix, so the adhered columns are to be separated and also text parts are to be removed. The Excel trick to do these tasks is described here. Click on the downward arrow on the *Paste Options* tag that appears nearby the pasted data (it has a suitcase icon shape). By clicking *Use Text Import Wizard* in the *Original data type* section, select *Fixed width* option. Click the next button. In the *Data preview section* you can separate the adhered columns which could not be recognized by Excel as distinct columns. Check for the possible errors in the lower rows. Then by right clicking on the selected text parts and selecting delete option it is possible to eliminate texts besides *shifting the cells up*. Finally the *matrix* is ready to be pasted to MATLAB *variable editor* to be saved as `MATRIX` in a MAT-file.

To transform the stresses in order to be compared with that of MMC method the following M-file is developed:

```
%% A MATLAB M-file to transform and plot ANSYS-extracted nodal stresses
%-----------------------------------------------------------------------------
%Before running the code...
%the MATRIX MAT-file is to be imported to Workspace!
List=MATRIX;
%The List matrix has 5 columns.
%The 1st column includes x coordinate of the path nodes.
%The 2nd column includes y coordinate of the path nodes.
%The 3rd column includes Sigma_x value at the path nodes.
%The 4th column includes Sigma_y value at the path nodes.
%The 5th column includes Sigma_xy value at the path nodes.
LL=length(List);
List(:,3:5)=List(:,3:5)/10^6;%Convert stress units from Pa to MPa
GS=zeros(LL,6);%Geometry and (transformed) Stress matrix
for i=1:LL
    %Geometrical parameters:
    GS(i,1)=sqrt(List(i,1)^2+List(i,2)^2);%Radial coordinate of nodes
    GS(i,2)=atan(List(i,2)/List(i,1));%Angular coordinate of nodes
    GS(i,3)=GS(i,2)-pi/2;%Stress transformation angle (negative)
    %Transformed stresses:
    %Sigma_r
    GS(i,4)=1/2*(List(i,3)+List(i,4))...
            -1/2*(List(i,3)-List(i,4))*cos(2*GS(i,3))...
            -List(i,5)*sin(2*GS(i,3));
    %Sigma_theta
    GS(i,5)=1/2*(List(i,3)+List(i,4))...
             +1/2*(List(i,3)-List(i,4))*cos(2*GS(i,3))...
             +List(i,5)*sin(2*GS(i,3));
    %Sigma_rtheta
    GS(i,6)=-1/2*(List(i,3)-List(i,4))*sin(2*GS(i,3))...
```

```
             +List(i,5)*cos(2*GS(i,3));
end
GS(:,2)=-GS(:,2);%Due to inversion of y-axis direction in ANSYS
                 %(in the MMC method y-axis is assigned downwards)

fig1=figure(1);
handle1=axes('fontsize',25);
set(fig1,'CurrentAxes',handle1)
%Sigma_r
plot(GS(:,2)*180/pi,GS(:,4),'-.red','LineWidth',3)
hold on
%Sigma_th
plot(GS(:,2)*180/pi,GS(:,5),'green','LineWidth',3)
hold on
%Sigma_rth
plot(GS(:,2)*180/pi,GS(:,6),':blue','LineWidth',3)
hold on
grid on
xlabel('\theta^{\circ}','fontsize',30)
ylabel('Stress (MPa)','fontsize',30)
set(gca,'XTick',-90:5:-45,'YTick',-20:5:30)
handle2=legend('\sigma_r','\sigma_\theta','\sigma_{r\theta}',...
                'Location','Northwest');
set(handle2,'fontsize',30);
%-----------------------------------------------------------------------------
```

The code results are shown in Figure 3.6 for a sample case together with the stress components calculated by the MMC method.

E.6 Calculating SIFs via displacement extrapolation method

To use *displacement extrapolation method* [11] offered by ANSYS to calculate SIF values [12], there are three steps to be taken after *the solution is done*. The method is limited to linear elastic problems with a homogeneous, isotropic material near the crack region. Before starting to take the steps, plot the deformed shape of the body by commanding:

```
ANSYS Main Menu>General Postproc>Plot Results>Deformed Shape
```

select the *Def shape only* option. Then *the first step* is to define a local crack-tip coordinate system:

```
ANSYS Utility Menu>WorkPlane>Local Coordinate Systems>Create Local CS
>By 3 Nodes
```

the picker pallet appears. Three nodes should be selected to define a local coordinate system positioned at the crack tip. These nodes are to be selected in a certain order. First of all, pick the crack-tip node. ANSYS perceives this as determination of the local coordinate system

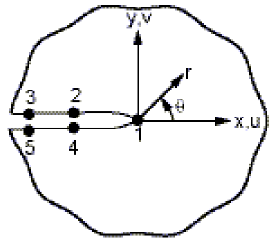

Figure E.4: The local x-y coordinate system and the path definition order

origin. Secondly, pick the closest node in the direction of (here tangential to) the crack surface at the crack tip. This will assign the local x-axis. Thirdly, pick the nearest node to the local origin in the direction perpendicular to the crack surface at the crack tip which specifies the local y-axis. Be careful not to choose the nodes in an arbitrary order.

In *the second step* a *path* is defined along the crack surface(s):

`ANSYS Main Menu>General Postproc>Path Operations>define Path>By Nodes`

again the first to be picked is the node at the crack-tip. A total number of five nodes are to be picked in the order shown in the Figure E.4. In the opening dialog box name the defined path.

Finally, in *the third step* calculate the SIF values by commanding:

`ANSYS Main Menu>General Postproc>Nodal Calcs>Stress Int Factr`

In the opening *stress Intensity Factor* dialog box, at the *KPLAN* field from the drop-down menu select *Plane stress* and at the *KCSYM* field select *Full-crack model*. Note that the symmetry concept aimed in the other option of the menu has nothing to do with the stress symmetry according to which only half of the beam is considered. Pressing the *Ok* button *KCALC* window displays SIF values (as *KI* and *KII*), plus some other details such as the path node numbers and mechanical properties of the body.